VALIDATION OF CReSIS SYNTHETIC APERTURE RADAR PROCESSOR AND OPTIMAL PROCESSING PARAMETERS

By

Logan Sanders Smith

Submitted to the graduate degree program in Electrical Engineering and the Graduate Faculty of the University of Kansas in partial fulfillment of the requirements for the degree of Master of Science.

_____

Chairperson Dr. John Paden

_____

Dr. Carl Leuschen

_____

Dr. Christopher Allen

Date Defended: 9/8/2014

The Thesis Committee for Logan Sanders Smith

certifies that this is the approved version of the following thesis:

VALIDATION OF CReSIS SYNTHETIC APERTURE RADAR PROCESSOR AND OPTIMAL PROCESSING PARAMETERS

_____

Chairperson Dr. John Paden

Date approved: 9/8/2014

ABSTRACT

Sounding the ice sheets of Greenland and Antarctica is a vital component in determining the effect of global warming on sea level rise. Of particular importance are measurements of the bedrock topography of the outlet glaciers that transport ice from the ice sheet's interior to the margin where it calves into icebergs, contributing to sea level rise. These outlet glaciers are difficult to sound due to crevassing caused by the relatively fast movement of the ice in the glacial channel and higher signal attenuation caused by warmer ice. The Center for Remote Sensing of Ice Sheets (CReSIS) uses multi-channel airborne radars which employ methods for achieving better resolution and signal-to-noise ratio (SNR) to better sound outlet glaciers. Synthetic aperture radar (SAR) techniques are used in the along-track dimension, pulse compression in the range dimension, and an antenna array in the cross-track dimension.

CReSIS has developed the CReSIS SAR processor (CSARP) to effectively and efficiently process the data collected by these radars in each dimension. To validate the performance of this processor a SAR simulator was developed with the functionality to test the implementation of the processing algorithms in CSARP. In addition to the implementation of this simulator for validation of processing the data in the along-track, cross-track and range dimensions, there are a number of data-dependent processing steps that can affect the quality of the final data product. CSARP was tested with an ideal simulated point target in white Gaussian noise. The SNR change achieved by range compression, azimuth compression, array combination with and without matched filtering, and lever arm application were all within .2 dB of the theoretical expectation. Channel equalization, when paired with noise-based matched filtering, provided 1-2 dB of gain on average but significantly less than the expected gain. Extending the SAR aperture length to sound bedrock will improve the along-track resolution, but at the expense of SNR. Increasing the taper of a window in the fast-time and slow-time will slightly improve the SNR of the data. Changing the relative permittivity used to process the data improved the resulting SNR by no more than 0.025 dB for the test dataset.

ACKNOWLEDGMENTS

First I would like to thank my wife, Sasha, for gifting me with so much love and support in my pursuit of my Master's degree. This would not be possible without her tolerance of my late nights and long hours, and bringing me food to sustain me. I would also like to thank my family for their continued support as the years stretched long. They kept me grounded during some hard times.

Thanks to my incredible advisor Dr. John Paden whose tireless work in editing and educating have made this thesis possible. His dedication is unparalleled. Thank you for fielding my questions both about research and about life. Without his help I would be a fraction of the researcher I am today.

Thank you to Dr. Gogineni for giving me so many wonderful opportunities to learn and travel. I am grateful for all the support and guidance he provided for me during my time here. I appreciate his candor and sense of humor as much as his intelligence and leadership.

Thank you to Dr. Leuschen and Dr. Allen for serving on my thesis committee. They helped me understand my thesis in a new light and how to improve it.

Thank you to all the CReSIS staff, faculty, and students for their support and friendship; especially to Anthony Hoch, Cameron Lewis, and Theresa Stumpf for talking through ideas with me and generally being good friends and people. I have really enjoyed being a part of CReSIS and will remember my time here fondly.

Contents

1. Introduction

1.1. Motivation

The scientific community agrees the average global temperature on Earth is steadily rising and will continue to rise under current conditions. This warming will affect aspects of modern culture, economics, politics, defense, and life in general in a number of ways. The most direct is the reclamation of land by rising sea level caused by the melting of the ice sheets. To predict the rate of melt, ice sheet modelers build simulations that convert knowledge about ice sheet dynamics and current ice sheet properties such as mass, makeup, and velocities into forecasts of sea level rise. While ice sheet dynamics have been studied both through models and in the field for many years, there are still portions of the Greenland and Antarctica ice sheets that have unmeasured properties vital to the ice sheet models. Two properties of prime importance are ice thickness and bedrock elevation. Ice thickness provides measurements of the volume of the ice sheet and is used in the ice sheet mass balance flux-gate method and bedrock elevation contributes to ice modeling efforts to determine where the ice will be moving and how fast. This information is used by modelers to calculate the contribution of ice sheets to sea level rise.

While much of Greenland's and parts of Antarctica's interior have been well mapped, they are relatively stable compared to the edges of each ice sheet. Outlet glaciers are special because they enable relatively rapid transportation of ice from an ice sheet's interior to the glacier calving front where the ice can calve off into icebergs, and eventually melt to create sea level rise. Many of these outlet glaciers have significantly increased velocity over the past two decades making a comprehensive understanding of their structure imperative.

1.2. Background

Many of the properties that make outlet glaciers important for ice sheet modeling also make them difficult to sound. Fast flowing ice is warmer than inland ice, which increases attenuation of the radar signal, and more crevassed, which changes the signal scattering properties. In addition, surface scattering from the channel walls and crevassed surface can overlay a strong clutter return on top of a weak bedrock return, making ice thickness measurement impossible.

Synthetic aperture radar and antenna arrays can be used to overcome some of these problems. In the direction of the radar platform's motion (along-track dimension) synthetic aperture radar techniques can be used to improve azimuth resolution. Perpendicular to the radar platform's motion (cross-track dimension) an antenna array will radiate more energy at the target and allow the use of beam-steering techniques to reduce clutter. In the range dimension increased bandwidth can be used to attain higher range resolution and when combined with pulse compression allows the signal power incident on the target to remain unchanged.

Implementation of these techniques requires advanced processing methods to make use of the collected data. A suite of functions to handle the processing of the data in the range, along-track,

and cross-track dimensions as well as organize the data for faster processing is a necessity, especially with large data sets. Researchers at the Center for Remote Sensing of Ice Sheets (CReSIS) have developed such a software suite using the MatLab coding environment to process data collected by CReSIS built radars in Greenland and Antarctica, including a number of fast-flowing glaciers in both areas.

1.3. **Objectives**

The CReSIS Synthetic Aperture Radar Processor (CSARP) is designed to fully process data collected by CReSIS radars. In order to obtain the most information from data collected from fast-flowing glaciers the algorithms in CSARP must be implemented properly and optimal processing parameters used. We wanted to create a radar simulator to validate the implementation of the algorithms used for range compression, azimuth compression, and array processing in CSARP. We also wanted to verify the functioning of the antenna lever arm application and the matched filtering of receiver elements with different noise powers.

To maximize the signal-to-noise ratio (SNR) of the resulting data we want to correct the phase, amplitude, and time delay errors introduced in the receive chain connected to each receive antenna. To do this we used a data dependent method to measure channel equalization coefficients that are applied to the data. We also wanted to look at the effects of SAR aperture length, fast-time and slow-time windowing, and relative permittivity on the final SNR of processed data.

1.4. **Organization**

There are six sections in this thesis. The first section outlines the motivations for this work and the research objectives. The second section details the design and implementation of the radar simulator used to validate CSARP. The third section describes the theory behind each step in CSARP and the application of simulated data to validate its implementation. The fourth section discusses the need for correcting the phase and amplitude errors between receiver channels to obtain the best SNR, a method for estimating these errors, and the correction of these errors. This section also includes an application of matched filtering to field-collected data with different noise levels and an analysis of the benefits and drawbacks of coherently combining the full 15-element array from the CReSIS 2011 Greenland P3 campaign for nadir sounding. Section five looks at the advantages and disadvantages of changing several important processing parameters. First of all, the trade-off between resolution and SNR when extending the SAR aperture length for point and distributed targets is discussed. Next, the effects of windowing, in the range and along-track dimensions, on target widening and SNR are examined. Finally, we look at the effect of changing the dielectric constant on SNR. The sixth section contains a summary of the results in this thesis and outlines recommendations for future work.

2. Radar Simulator

A radar simulator is an invaluable tool for breaking down the analysis of a system. Simulated data can be totally defined by the user to validate processes or expose errors. It can also be useful in developing advanced processing techniques and gaining a better understanding of issues in the collection of data.

We have built a basic ice-penetrating radar simulator adapted from one written by Dr. Jilu Li for his Ph.D. dissertation [1]. It creates data compatible with the CReSIS Synthetic Aperture Radar Processor (CSARP) to validate each component of the processing chain. The simulator includes the functionality to create radar data with user defined radar parameters, multiple antennas, multiple waveforms, motion error, and receiver channel imbalances. See Appendix A for operating instructions.

2.1. Files and File Formats

In order to test the CSARP processing chain the simulator output is created to be ingested into CSARP identically to real science data. This requires several auxiliary files to be created in addition to the simulated radar data. A GPS/INS file allows for user defined platform trajectories, a CSARP records file stores all the loading and processing parameters, and a CSARP frames file stores information about how to split the raw data into output data frame images. The simulator writes the data as 16-bit unsigned integer binary files, identical to those produced by CReSIS's Multichannel Radar Depth Sounder (MCoRDS) so that they are easily ingested into CSARP.

2.2. Geometry

We use the flight coordinate system (FCS) with the direction of motion in the positive x-direction, the positive z-direction is the projection of the normal to the WGS-84 ellipsoid on to the surface orthogonal to the x direction and pointing away from the Earth's center, and the positive y-direction is made to form a right handed coordinate system which means that it points out the left wing of the aircraft as shown in Figure 2-1.

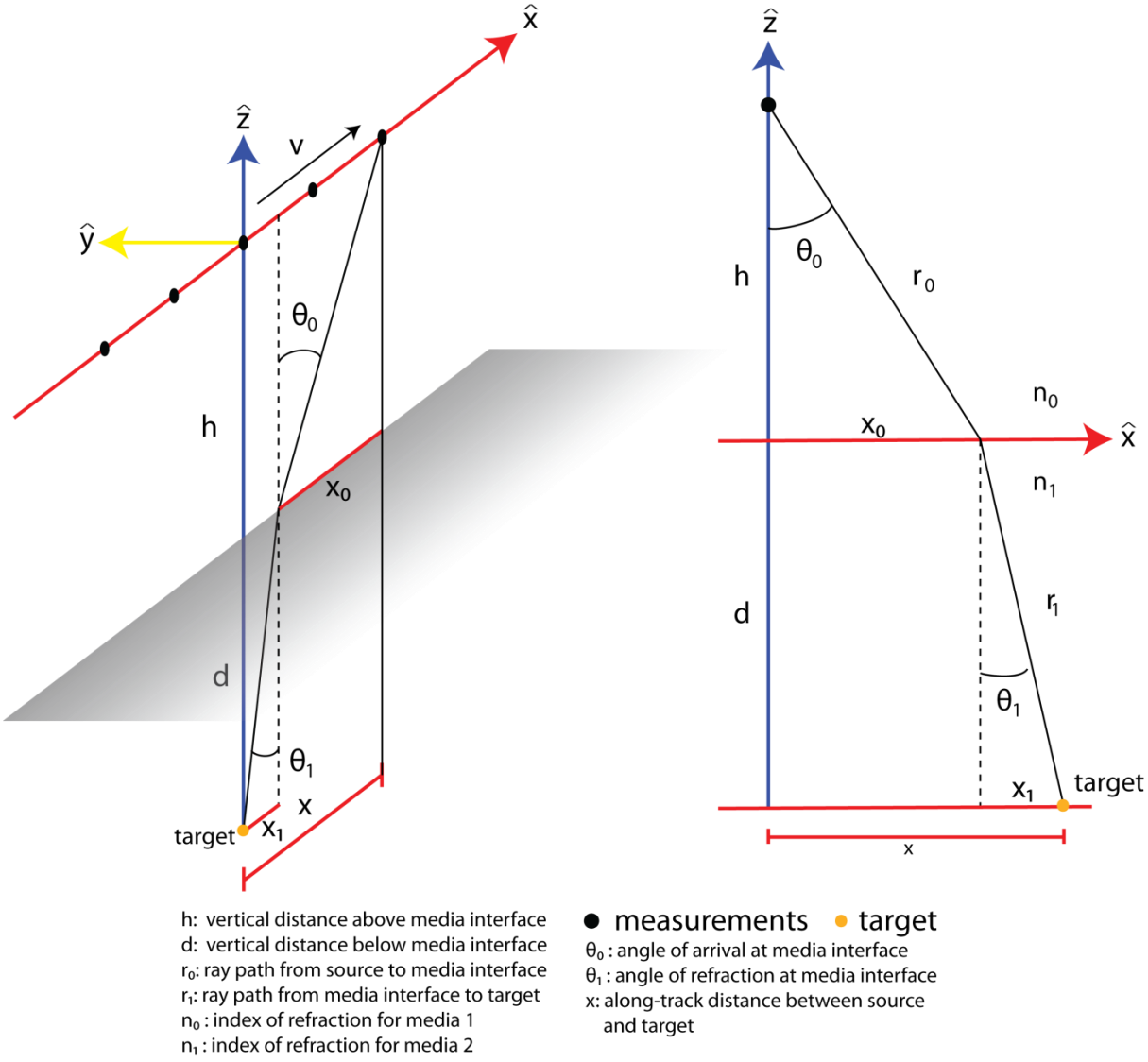

Figure 2-1: Radar system geometry.

In the simulated image space the extent in the z-dimension (depth) is a user defined parameter and the extent in the x-dimension (along-track distance) is twice the maximum along-track beamwidth value to capture the full point scatter response.

2.2.1. Simulated Trajectory

Simulated trajectory data are created by assuming the platform is travelling due north somewhere in the vicinity of Greenland. The distance covered in the trajectory file (gps_YYYYMMDD.mat) is determined by holding the starting point stationary while iteratively moving the end point due north until the trajectory matches the user defined path length. The roll, pitch, and heading vectors default to all zeros but can be changed by the user. A roll and

pitch of zero implies level flight and a heading vector of zero implies the platform is pointed towards north.

2.2.2. Phase Center of Measurement

The GPS data locations are at the trajectory reference location, but this is generally not where the radar phase center is. The GPS data must be updated to reflect the actual location of the measurement's phase center. We collect measurements in bistatic mode which means the transmit and receive antennas are not collocated. The phase center of a bistatic measurement is the location which yields the same results as when a monostatic setup is used. In other words, if the transmit and receive antennas were physically collocated at the phase center the results would be the same as for the bistatic measurement. Note that *same* results is used loosely here, since there is in fact a small discrepancy anytime the bistatic baseline or separation between transmit and receive antennas is greater than zero.

Each measurement is a combination of transmit and receive elements and the phase center for the measurement is the center of gravity of these elements **[2]**. To determine the position or phase center of the measurement, we need to know each element's lever arm to the reference point that the trajectory is processed to. The reference point is often a GPS antenna or the INS unit, but may be elsewhere. The transmit elements are described by a combined phase center because they are all used to simultaneously transmit while each receive antenna receives signals separately. The lever arm for each radar and platform is stored in the lever_arm.m Matlab function. This function contains the 3D position of the trajectory reference location and the phase center for each antenna element in the aircraft body coordinate system. The body coordinate system is a right handed rectangular coordinated system with +x in the direction of motion, +y out the right wing, and +z down. The lever arm geometry is shown in Figure 2-2. The phase center for each measurement is defined as

$$pc(x,y,z) = \frac{\left(LA_{rx}(x,y,z) + \frac{dot(LA_{tx}(x,y,z), w_{tx})}{sum(w_{tx})}\right)}{2}, \quad (1)$$

where $LA_{rx}(x,y,z)$ is the 3D position of the receive phase center, $LA_{tx}(x,y,z)$ is the 3D position of the combined transmit phase center, and W_{rx} are the transmit antenna weights.

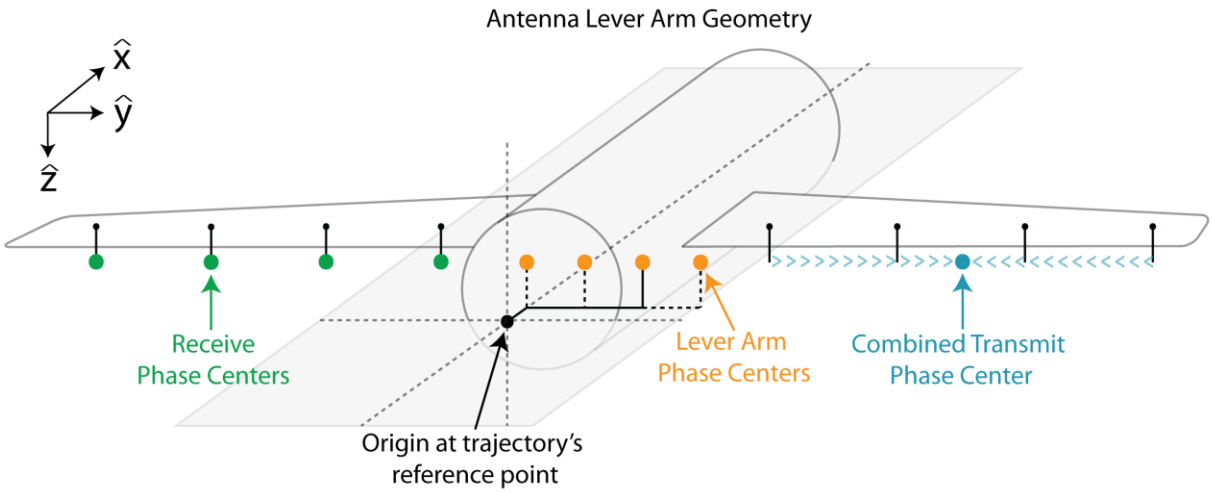

Figure 2-2: Antenna lever arm diagram.

2.3. Propagation Model

2.3.1. Signal Model

We assume the recorded signal is of the form

$$x(t) = s(t) + n(t), \tag{2}$$

where *x(t)* is the recorded signal, *s(t)* is the transmitted signal, and *n(t)* is uncorrelated zero-mean Gaussian noise. The transmitted signal is a chirp pulse of the form

$$s_{tx}(t) = A(t) \cdot exp(j2\pi f_0 t + j\pi\alpha t^2), \tag{3}$$

where

$\alpha = \frac{B}{T_{pd}}$ is the chirp rate,
B is the signal bandwidth,
T_{pd} is the signal pulse duration,
$A(t)$ is the envelope, and
f_0 is the start frequency of the chirp.

The transmitted signal scatters off the target and returns to the radar with a delay of $t_d(\vec{r}, \vec{r_s})$ where $\vec{r}$ is the position of the measurement phase center and $\vec{r_s}$ is the position of the target. The time delay is defined in Section 2.3.2. Superimposed on this, is the noise signal $n(t)$ which is modeled as thermal noise or a white Gaussian random process (Equation (4)). The noise power is derived in section 2.5.2. The probability density function of the noise is stationary and is given by

$$f_n(n) = \frac{1}{\sigma_N\sqrt{2\pi}} e^{-\frac{n^2}{2\sigma_N^2}}, \tag{4}$$

where σ_N is the noise variance.

The received signal has the form

$$s_{rx}(t) = s_{tx}\left(t - t_d(\vec{r}, \overrightarrow{r_s})\right) + n(t),$$
$$s_{rx}(t) = A\left(t - t_d(\vec{r}, \overrightarrow{r_s})\right) \cdot exp\left(j2\pi f\left(t - t_d(\vec{r}, \overrightarrow{r_s})\right) + j\pi\alpha\left(t - t_d(\vec{r}, \overrightarrow{r_s})\right)^2\right) + n(t) \quad (5)$$

Although signal attenuation factors are not included in the CSARP validation simulation data set, the ability to add them exists in the simulator. Currently these include target cross section, spherical spreading loss, and ice attenuation.

MatLab employs a global random number generator stream and this stream can be accessed using the RandStream constructor. To guarantee uniform, but still pseudo-random, noise data RandStream is seeded with the same value before the noise signal is created each time the simulator is run. This helps to improve the consistency of the noise portion of the output data between simulated data sets by ensuring the noise data are still random over a single simulated data set but identical between data sets (useful when comparing different methods of collection).

2.3.2. Refraction Model and Time Delay

A two-media refraction model is used to calculate the two-way travel time of the radar signal at each phase center $\vec{r}$ of the simulated data. The height of the phase center above the interface h, the depth of the target below the interface d, and along-track displacement between the receiver and target x are all known. The along-track position of the intersection of the signal's ray path with the air-ice interface can be calculated using a root solver of the fourth-order equation derived from Snell's law at the air-ice interface. This equation is derived in appendix B. The geometry can be seen in Figure 2-1. To get the signal's time delay t_d for the corresponding along-track distance we can simply use the Pythagorean Theorem to determine the slant range from the radar to the air-ice interface in air, r_{air}, and from the interface to the target in ice, r_{ice}, then convert these ranges into time using an ice dielectric, ϵ_r, of 3.15 as follows

$$r_{air}(x) = \sqrt{h^2 + x_0^2}, \quad (6)$$

$$r_{ice}(x) = \sqrt{d^2 + x_1^2}, \quad (7)$$

and

$$t_d(x) = \frac{2\left(r_{air}(x) + sqrt(\varepsilon_r) \cdot r_{ice}(x)\right)}{c}. \quad (8)$$

For each record a linear chirp is created over the entire time axis then phase shifted by the time delay for that record. The chirp is then masked to the pulse duration with a Tukey window (i.e. $A(t)$ is a Tukey window of duration T_{pd}) to reduce sidelobes and an angle-of-arrival mask is used to limit the target response to the effective SAR aperture. Multiple targets can be summed up because of the principle of superposition where we assume that the scattering between targets can be ignored.

2.3.3. Channel Equalization Errors

Channel equalization errors perturb the signal for each channel to simulate the mismatches caused by channel to channel variations in the receive chains. There are separate coefficients for time delay, phase, and amplitude mismatches. Channel equalization is discussed further in section 4.

The channel equalization coefficients are applied after the noise signal is added. The time delay errors are applied via a phase shift in the frequency domain (Equation (9)) while the amplitude and phase errors are applied via a scaling factor and phase shift in the time domain (Equation(10)).

$$s_{offset,1}(t) = \int_{-\infty}^{\infty} S(f) e^{-j2\pi f EQ_{td}} e^{j2\pi f t} df, \tag{9}$$

$$s_{offset}(t) = EQ_{chan} \cdot s_{offset,1}(t), \tag{10}$$

$$EQ_{chan} = 10^{\frac{EQ_{amp}}{20}} e^{jEQ_{\phi}\frac{\pi}{180}}, \tag{11}$$

where
$S(f)$ is the frequency transform of $s(t)$,
EQ_{td} is the time delay mismatches in seconds,
EQ_{amp} is the power mismatches in dB, and
EQ_{ϕ} is the phase mismatches in degrees.

2.4. ADC

To make the simulator more compatible with CSARP the output is written as a binary file identical to the CReSIS analog to digital converter (ADC). The ADC is modeled off those currently used in the CReSIS radars which are 14-bit with a 2 V_{pp} full-scale voltage range. Assuming the ADC has an ideal effective number of bits (ENOB) of 14-bits the quantization noise floor is

$$20\ log_{10}\left(\frac{2}{2^{bits+1}}\right) = -84\ dBW, \tag{12}$$

where $bits$ is the number of ADC bits.

In the quantization step, the data is first checked for values larger than half the full-scale voltage range (1 V_{pp}) and a warning is displayed if there are clipped values. Then the data is shifted so all values fall between 0 and 16383 (2^{14}-1) and can be written as 16-bit unsigned integers.

To reduce the data rate in the actual data acquisition system, coherent integrations, also called presums, are performed in hardware to reduce the necessary write speed. Each time the number of presums is doubled the data requires another output bit to be fully recorded. Because the ADC outputs 14-bit values and the data are written to 16-bit values there are two extra bits that

can be used before a data value must be truncated in some way. These two extra bits equate to $2^2 = 4$ available presums. After 4 presums a decision must be made to shift the data to the left or right by one bit. Since the data is written in big-endian format, shifting to the left removes the most significant bit and shifting right removes the least significant bit. The assumption made is that the noise is sufficiently large so that dropping the least significant bits does not affect dithering even after presumming. An example of the process can be found in appendix C.

2.5. Link Budget and Power Levels

The receive power of the reflected signal can be calculated using the radar range equation (Equation (13)). This includes losses due to spherical spreading, propagation loss, and target scattering. In this validation scenario no losses are enabled in the simulated data but the ability to include losses is available in the simulator [3].

$$P_R = \frac{P_T \cdot G^2 \lambda^2 \sigma L}{(4\pi)^3 \left(R_{air} + \frac{R_{ice}}{\sqrt{\epsilon_r}}\right)^4}, \tag{13}$$

where

P_R is the received power,
P_T is the transmit power,
G is the antenna gain,
σ is the radar cross section,
R_{air} is the range in air,
R_{ice} is the range in ice, and
L is the extinction loss.

2.5.1. Noise Power

The noise is modeled as Gaussian white noise and is added to the data signal. The system noise power is given by:

$$P_{thermal} = 10\, log_{10}(kTB) + F = -127.3 \text{ dB}, \tag{14}$$

where

$k = 1.3806488x10^{-23}$ JK^{-1} is Boltzmann's constant,

$T = 290$ K is the approximate system temperature,

$B = 30$ MHz is the receiver's noise bandwidth, and

$F = 1.91$ dB is the system's noise figure.

To create this during simulation, we use additive white Gaussian noise at the sampling frequency (a 1 GHz clock divided by 9 or $111.\overline{1}$ MHz). This means that the total noise power is actually -121.6 dB and higher than the actual system. Pulse compression acts like a band pass filter

removing thermal noise outside of the band. This will drop the noise floor back to its expected level after range compression.

2.5.2. Signal Power

The simulated ADC has a peak-to-peak voltage limit of 2V so a signal with amplitude 1V peak-to-peak can easily be digitized. Assuming a characteristic system impedance of 1 Ω, setting the signal peak-to-peak voltage, V_{pp}, to 1 V requires a peak transmit power of $P_T = P_{avg} = \frac{|V_{rms}|^2}{Z_0} = \frac{|V_{pp}|^2}{8Z_0} = 125$ mW (-9.03 dB) per channel. This low transmit power is used since losses are ignored in the simulation. The physical CReSIS radars use significantly more power, for instance the 2011 Greenland P3 used a transmit power up to 1050W spread over 7 transmit antennas.

This makes the signal to noise ratio (SNR) of the raw simulated data

$$SNR_{raw} = -9.03\ dB\ +\ 121.6\ dB\ =\ 112.57\ dB.$$

2.5.3. Receiver Gain

Once the signal with noise reaches the ADC the quantization noise floor dominates. The quantization noise floor for the ADC is -84 dB from Equation (12), 37 dB higher than the thermal noise floor. To avoid losing small returns to the quantization floor we add a receiver gain to the noise power which includes the 37 dB plus a 10 dB buffer plus another 3 dB to compensate for removing the imaginary part of the signal when writing the simulated data to file. This gives a final simulated noise power of 71.28 dB.

Since we cannot exceed 2 V_{pp} for the received signal the receiver gain is only applied to the noise signal making the SNR_{raw} = -9.03 dB + 71.28 dB = 62.25 dB.

2.6. Simulated Data

The purpose of the simulator for this thesis is to create data that can be used to verify the functioning of the CSARP. The results of the processed simulated data will be compared to theoretical calculations and the CSARP algorithms will be validated based on that comparison. To have confidence in these results we start with the simplest data possible and add complexity from there.

We start with a simple point target in white Gaussian noise to validate range compression, azimuth compression, and array processing. Next we added the lever arm offset and finally channel equalization. The results of these tests are presented in section 3.

A sample of a point target with additive white Gaussian noise is shown in Figure 2-3.

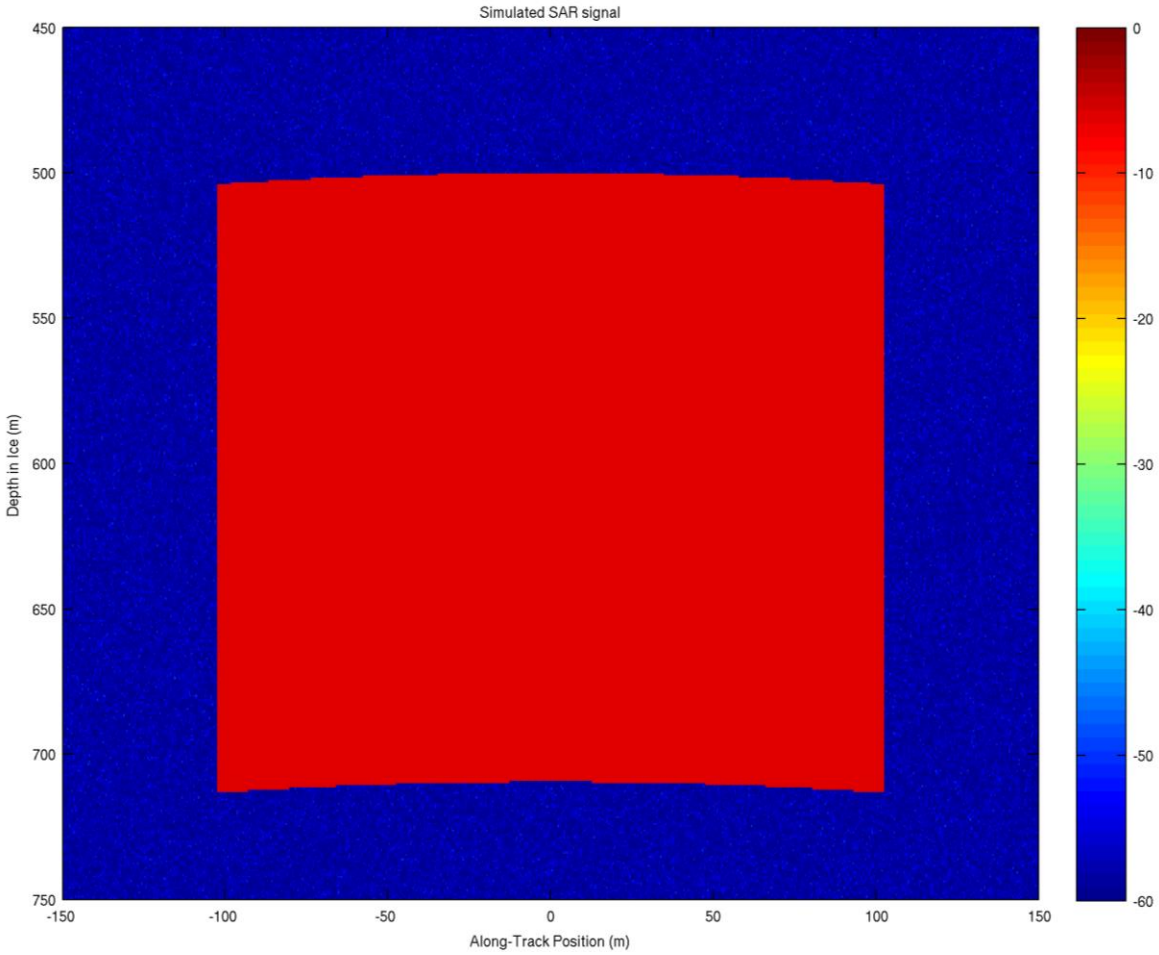

Figure 2-3: Simulated point target in raw collected form. The color axis is relative power in dB.

3. CReSIS Synthetic Aperture Radar Processor (CSARP)

CSARP is a set of MATLAB scripts used to process raw CReSIS radar data and organize the outputs. There are six steps in the CSARP process with the first three creating auxiliary files and the final three processing the data in the range, azimuth, and cross-track dimensions respectively. The purpose of CSARP is to take the data from its raw state and produce the best possible results in terms of ice thickness measurements (resolution, SNR, clutter reduction).

3.1. Data Collection

The CReSIS radar depth sounders transmit a chirped pulse $s_{tx}(t)$ (Equation (3)) to sound the bedrock of the Greenland and Antarctic ice sheets. The range resolution of an impulse radar is defined by the pulse duration of the transmitted signal and is $\sigma_r = \frac{1}{2} c T_{pd}$ where c is the speed of light in a vacuum and T_{pd} is the pulse duration. In the case where the transmitted signal is a chirped pulse, the range resolution, after pulse compression, is $\sigma_r = \frac{c}{2B}$ where B is the signal bandwidth. Using pulse compression allows more energy to be transmitted without reducing the range resolution or increasing the peak power. Since the fall of 2009, the transmit signal has also been windowed in the time domain with a 20% Tukey window to reduce range sidelobes caused by the sudden transitions of the envelope in a standard chirped pulse. Range sidelobes will be discussed further in section **5.2.1**.

Traditional radars use real aperture radar (RAR) methods to collect data. This means that along-track resolution is determined by the antenna's beamwidth in that dimension which is determined by the physical size of the (real) antenna. The aperture length is inversely proportional to the along-track resolution (i.e. a longer aperture is required for finer resolution). If the desired resolution requires an aperture that is longer than is physically feasible for the platform (which is typically the case for airborne or spaceborne radars), the data can be collected using the synthetic aperture radar (SAR) method. SAR requires that the target is static and platform motion to move the antenna along a synthetic aperture. The idea is to use a small antenna and move it, while taking measurements, along the required aperture length. In processing, we then combine these individual measurements to *synthesize* a longer aperture. In SAR both the transmit and receive phase centers move so the phase shift associated with a target at two adjacent antenna positions is the product of the two-way, rather than one-way, travel time, making the resolution for a given aperture twice as fine as that of RAR. This gives SAR the advantage of requiring only half the aperture length of RAR to achieve the same resolution. Figure 3-1 shows a comparison of RAR and SAR data collection. In RAR, only a single measurement is needed for each target. In SAR, many measurements of the same target are taken. Figure 3-2 shows what a single point target looks like when collected using the SAR method along a straight line; the time delays associated with the geometry cause the point target to look like a hyperbola with the vertex occurring at the position of closest approach between the radar and the target. For a linear trajectory, the energy reflected from a target is spread over adjacent records as a hyperbola and needs to be re-focused

during SAR processing to the target's actual location to achieve the maximum gain in SNR and the desired resolution.

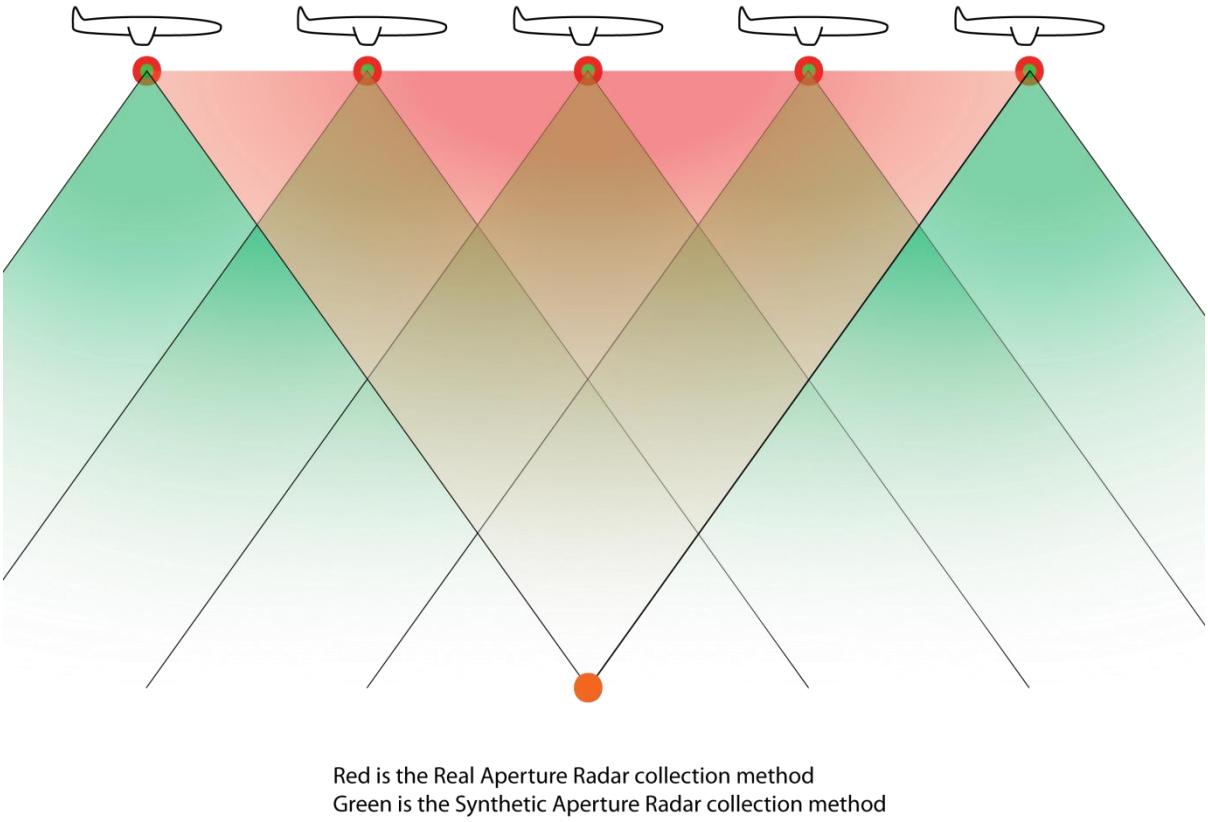

Figure 3-1: Synthetic aperture radar versus real aperture radar geometry. The synthetic aperture has half the beamwidth of the real aperture.

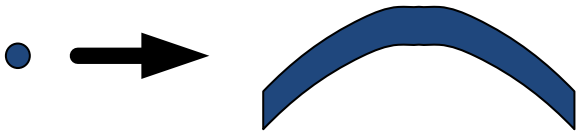

Figure 3-2: Point targets in the data space become thick hyperbolas in the raw phase history space.

3.2. Simulated Verification Data

The specific data simulated for CSARP verification is modeled after the 2011 Greenland Twin Otter mission MCoRDS settings.

Table 3-1: Radar parameters.

Parameter	Symbol	Value
Center Frequency	f_c	195 MHz
Sampling Frequency	f_s	$111.\overline{1}$ MHz
Pulse Type		Linear Chirp
Pulse Repetition Frequency	f_{PRF}	187.5 Hz
Noise Figure	F	1.91 dB
Temperature	T	290 K
Tx Antenna Weights		[1 1 1 1]
Rx Channels		4
ADC Full Scale Voltage		$2\ V_{pp}$
ADC Bits		14
Along-track Beamwidth		80°
Characteristic Impedance	Z_0	1 Ω

Table 3-2: Waveform parameters.

Parameter	Symbol	Value
Pulse Duration	T_{pd}	2.5 µs
Bandwidth	B	30 MHz
Start Frequency	f_0	180 MHz
Stop Frequency	f_1	210 MHz

Table 3-3: Platform parameters.

Parameter	Symbol	Value
Aircraft Velocity	v	60 m/s
Aircraft Altitude	h	500 m

Table 3-4: Scene parameters.

Parameter	Symbol	Value
Along-track sample size	$\Delta_x = \frac{v \cdot presums}{f_{PRF}}$	0.32 m
Scene along-track length		3556 m
Sample interval	Δ_t	9 ns
Sample start time	t_s	0 μs
Sample end time	t_f	50 μs
Number of fast-time samples	N_t	5500
Number of slow-time samples	N_x	11114
Number of samples in transmitted pulse	N_{tx}	278

3.2.1. Basic Simulation Parameters

Table 3-5: Simulation Parameters

Target depth:	500 m
Time delay errors:	[0 0 0 0]1E-9 s
Phase errors:	[0 0 0 0]°
Amplitude errors:	[0 0 0 0] dB
Noise floor mismatch:	[0 0 0 0] dB

3.3. Matched Filter

We define the matched filter to be the linear filter that maximizes the SNR of a known signal in correlated Gaussian noise. It correlates a copy of the transmitted signal with the received signal which creates a peak wherever the transmitted signal has reflected off a target. A derivation of the matched filter can be found in appendix D.

We assume the recorded signal is of the form

$$\boldsymbol{x} = \boldsymbol{G}\boldsymbol{s} + \boldsymbol{n}, \tag{15}$$

where $\boldsymbol{x} \in \mathbb{C}^{\boldsymbol{n}}$ is the recorded signal vector, $\boldsymbol{G} \in \mathbb{C}^{\boldsymbol{nxm}}$ is the steering matrix, $\mathbf{s} \in \mathbb{C}^{\mathbf{m}}$ represents the scattering strength of M targets, and $\boldsymbol{n} \in \mathbb{C}^{\mathbf{n}}$ is a random vector of correlated zero-mean Gaussian noise.

The steering matrix describes the matched filter coefficients. It represents the measured signal received from a unit strength target. For example, the steering matrix for cross-track measurements describes how the signal energy is applied to each of the antenna elements. For ideal isotropic antenna elements,

$$\boldsymbol{G} = e^{j\boldsymbol{k}^{\boldsymbol{H}}\boldsymbol{r}}, \tag{16}$$

where $\boldsymbol{k}$ is the wavenumber vector of the plane wave in question (magnitude $\frac{4\pi}{\lambda}$ and pointing in the direction of propagation) and $\boldsymbol{r}$ is an N by 3 matrix where the ith row corresponds to the ith 3 by 1 antenna lever arm offset ordered as $[x,y,z]^T$.

The signal and noise are assumed to be independent of each other. The additive noise has a covariance matrix $\boldsymbol{C} \in \mathbb{C}^{\boldsymbol{nxn}} = E\{\boldsymbol{n}\boldsymbol{n}^H\}$. All vectors and matrices are complex. The matched filter coefficients for a scalar signal ($\boldsymbol{G}$ is a single column represented by $\boldsymbol{g}$) are of the form

$$\boldsymbol{w} = \frac{\boldsymbol{C}^{-1}\boldsymbol{g}}{\boldsymbol{g}^H\boldsymbol{C}^{-1}\boldsymbol{g}}. \tag{17}$$

3.3.1. Special Cases

There are two special cases of the matched filter that are particularly applicable to our processing. A full derivation of the coefficients for each special case can be found in Appendix D.

3.3.1.1. Independent Noise

In the case where the noise for each sample is independent but not identically distributed, all off-diagonal elements of the noise covariance matrix will be zero and the correlation matrix is

$$\boldsymbol{C} = \begin{bmatrix} \sigma_1^2 & \cdots & 0 \\ \vdots & \ddots & \vdots \\ 0 & \cdots & \sigma_N^2 \end{bmatrix}, \tag{18}$$

where σ_i is the noise variance from channel i. The matched filter weights are then:

$$\boldsymbol{w} = \frac{1}{\sum_{i=1}^{N}|g|^2\sigma_i^{-2}}\begin{bmatrix} \sigma_1^{-2}g_1 \\ \sigma_2^{-2}g_2 \\ \vdots \\ \sigma_N^{-2}g_N \end{bmatrix}. \tag{19}$$

3.3.1.2. Independent and Identically Distributed (IID) Noise

In the case where the noise signal in each sample of the signal is independent and identically distributed (IID) the matched filter improves the SNR by a factor of N where N is the number of samples in the signal. This is the case for range and azimuth compression.

$$\boldsymbol{C} = \begin{bmatrix} \sigma^2 & \cdots & 0 \\ \vdots & \ddots & \vdots \\ 0 & \cdots & \sigma^2 \end{bmatrix} = \boldsymbol{I}_N\sigma^2, \tag{20}$$

where $\boldsymbol{I}_N$ is the N by N identity matrix. In this special case, the weights are

$$\boldsymbol{w} = \frac{\boldsymbol{g}}{\|\boldsymbol{g}\|}. \tag{21}$$

3.3.2. Expected SNR Gain from Matched Filtering

The matched filter coefficients are

$$\boldsymbol{w} = \frac{\boldsymbol{C}^{-1}\boldsymbol{g}}{\boldsymbol{g}^H\boldsymbol{C}^{-1}\boldsymbol{g}}. \tag{22}$$

The signal estimation is

$$\hat{\boldsymbol{s}} = \boldsymbol{w}^H\boldsymbol{x} = \boldsymbol{w}^H(\boldsymbol{G}\boldsymbol{s} + \boldsymbol{n}). \tag{23}$$

The signal power is

$$P_S = (\boldsymbol{w}^H\boldsymbol{g}\boldsymbol{s})^H(\boldsymbol{w}^H\boldsymbol{g}\boldsymbol{s}) = \frac{(\boldsymbol{g}^H\boldsymbol{C}^{-1}\boldsymbol{g})\boldsymbol{s}^H}{\boldsymbol{g}^H\boldsymbol{C}^{-1}\boldsymbol{g}}\frac{\boldsymbol{s}(\boldsymbol{g}^H\boldsymbol{C}^{-1}\boldsymbol{g})}{\boldsymbol{g}^H\boldsymbol{C}^{-1}\boldsymbol{g}} = \boldsymbol{s}^H\boldsymbol{s}. \tag{24}$$

The noise power is (see appendix D for full derivation)

$$P_N = E\{(\boldsymbol{w}^H\boldsymbol{n})^H(\boldsymbol{w}^H\boldsymbol{n})\} = \frac{\boldsymbol{g}^H\boldsymbol{C}^{-1}\boldsymbol{C}\boldsymbol{C}^{-1}\boldsymbol{g}}{(\boldsymbol{g}^H\boldsymbol{C}^{-1}\boldsymbol{g})^2} = \frac{\boldsymbol{g}^H\boldsymbol{C}^{-1}\boldsymbol{g}}{(\boldsymbol{g}^H\boldsymbol{C}^{-1}\boldsymbol{g})^2} = \frac{1}{\boldsymbol{g}^H\boldsymbol{C}^{-1}\boldsymbol{g}}. \tag{25}$$

If equal weights, which are optimal only for IID noise, are applied to the general case, the noise power is

$$P_{N-mismatch} = E\{(\boldsymbol{w}^H\boldsymbol{n})^H(\boldsymbol{w}^H\boldsymbol{n})\} = \frac{\boldsymbol{g}^H\boldsymbol{C}_{\boldsymbol{eq}}^{-1}\boldsymbol{C}\boldsymbol{C}_{\boldsymbol{eq}}^{-1}\boldsymbol{g}}{\left(\boldsymbol{g}^H\boldsymbol{C}_{\boldsymbol{eq}}^{-1}\boldsymbol{g}\right)^2}. \tag{26}$$

$\boldsymbol{C}_{\boldsymbol{eq}}^{-1} = \frac{1}{\sigma^2}\boldsymbol{I}$ is the covariance matrix for IID noise

$\sigma^2$is the noise power

$\boldsymbol{I}$ is the identity matrix

Assuming all signals have identical signal power implies the SNR gain from using the optimal matched filter coefficients as opposed to non-optimal equal weights is determined by the noise power alone as

$$SNR_{mf-gain} = \frac{P_{N-mismatched}}{P_N}. \tag{27}$$

3.4. CSARP Processing Steps and Verification

This section explains the steps used to process CReSIS data in CSARP, develops the theory for the expected gains from each step, and presents the results from the verification using simulated data.

3.4.1. Auxiliary Files

Steps 1-3 are for the creation of auxiliary files and will only be included here for completeness; they are 1) creation of vector files which contain basic information about the location in time and space of the first record of each raw data file, 2) creation of records files which contain all pertinent metadata for each record of the raw data, and 3) creation of frames files which contain

the raw data indexes that divide CSARP output files. The next step is for determining the height of the platform above the ice surface and creating range compressed-only data for use in quick analysis processes.

3.4.2. Range Compression via Matched Filtering

In order to improve range resolution and SNR, pulse compression theory is used when transmitting the radar signal. Pulse compression uses a chirped waveform on transmit to improve the bandwidth and thus the range resolution of the target response. The longer pulse duration allows more energy to be put on a target. To recover any targets the received signal is correlated with a reference signal which is typically a replica of the transmitted pulse (if available) or an ideal version of the transmitted pulse. The correlating signal used is the matched filter for the transmitted signal. Matched filter theory tells us this will provide the maximum SNR assuming the only noise present is Gaussian white noise. The matched filter weights for a signal with IID Gaussian noise and identical steering vectors is:

$$\boldsymbol{w} = \frac{\boldsymbol{g}}{\|\boldsymbol{g}\|} = \frac{1}{N} ones(1, N) \tag{28}$$

The effect is to compress the thick hyperbola seen in Figure 2-3 to a hyperbola as shown in Figure 3-3.

For a pulse of duration T_{pd} sampled at f_s with bandwidth B there are $N_{tx} = T_{pd} f_s$ samples in the transmitted pulse but only $N = T_{pd} B$ independent samples if the noise is restricted to the signal bandwidth. For the received signal each sample is correlated with the replica so the output is

$$y_{sig}[n] = \sum_{k=0}^{N-1} s^*[k] x[n+k] \tag{29}$$

where $x[k] = s[k] + n[k]$ and $s[k]$ is the signal. For an offset aligned with a target return at $n = 0$, the signal is

$$\begin{aligned} y_{sig}[0] &= \sum_{k=0}^{N-1} s^*[k] x[k] = \sum_{k=0}^{N-1} s^*[k](s[k] + n[k]) \\ &= \sum_{k=0}^{N-1} |s[k]|^2 + n[k] s^*[k]. \end{aligned} \tag{30}$$

Note that the correlation operation is equivalent to an inner product operation between two N length vectors. Assuming a constant envelope for the signal, IID noise, converting to vector notation, and using the fact that the signal is nonrandom, the signal to noise ratio relative to the individual sample signal power, P_s, and noise power, P_n,:

$$SNR = \frac{|\sum_{k=0}^{N-1}|s[k]|^2|^2}{|\sum_{k=0}^{N-1} n[k]s^*[k]|^2} = \frac{P_S^2 N^2}{E\{\boldsymbol{s}^H \boldsymbol{n}(\boldsymbol{s}^H \boldsymbol{n})^H\}}$$
$$= \frac{P_S^2 N^2}{\boldsymbol{s}^H E\{\boldsymbol{n}\boldsymbol{n}^H\}\boldsymbol{s}} = \frac{P_S^2 N^2}{\boldsymbol{s}^H \boldsymbol{C}\boldsymbol{s}} = \frac{P_S^2 N^2}{P_s P_n N} = \frac{P_s}{P_n} N \quad (31)$$

Then the SNR gain is N as compared to the original sample SNR of $\frac{P_s}{P_n}$.

3.4.2.1. Time-Bandwidth Product

The SNR gain from pulse compression can also be calculated using the time-bandwidth product which, as the name implies, is the product of the pulse duration and the signal bandwidth. This product is the number of samples, N, from the previous section or

$$N = T_{pd} B. \quad (32)$$

In the simulation, the raw data's noise power is $\frac{f_s}{B}$ higher than desired because the noise power is the full sampling bandwidth. The reported SNR for the raw data takes this into account so the value reported is the value for a noise bandwidth of B.

3.4.2.2. Simulation Expectation and Results

In the basic verification simulation the expected processing gain from Equation (32) is

$$2.5 \times 10^{-6} \cdot \ 30 \times 10^{6} = 75 = 18.75 \text{ dB}$$

The total expected SNR after range compression is

$$SNR_{rc} = 62.36 + 18.75 = 81.11 \ dB$$

The actual SNR is 81.26 dB as shown in Figure 3-6.

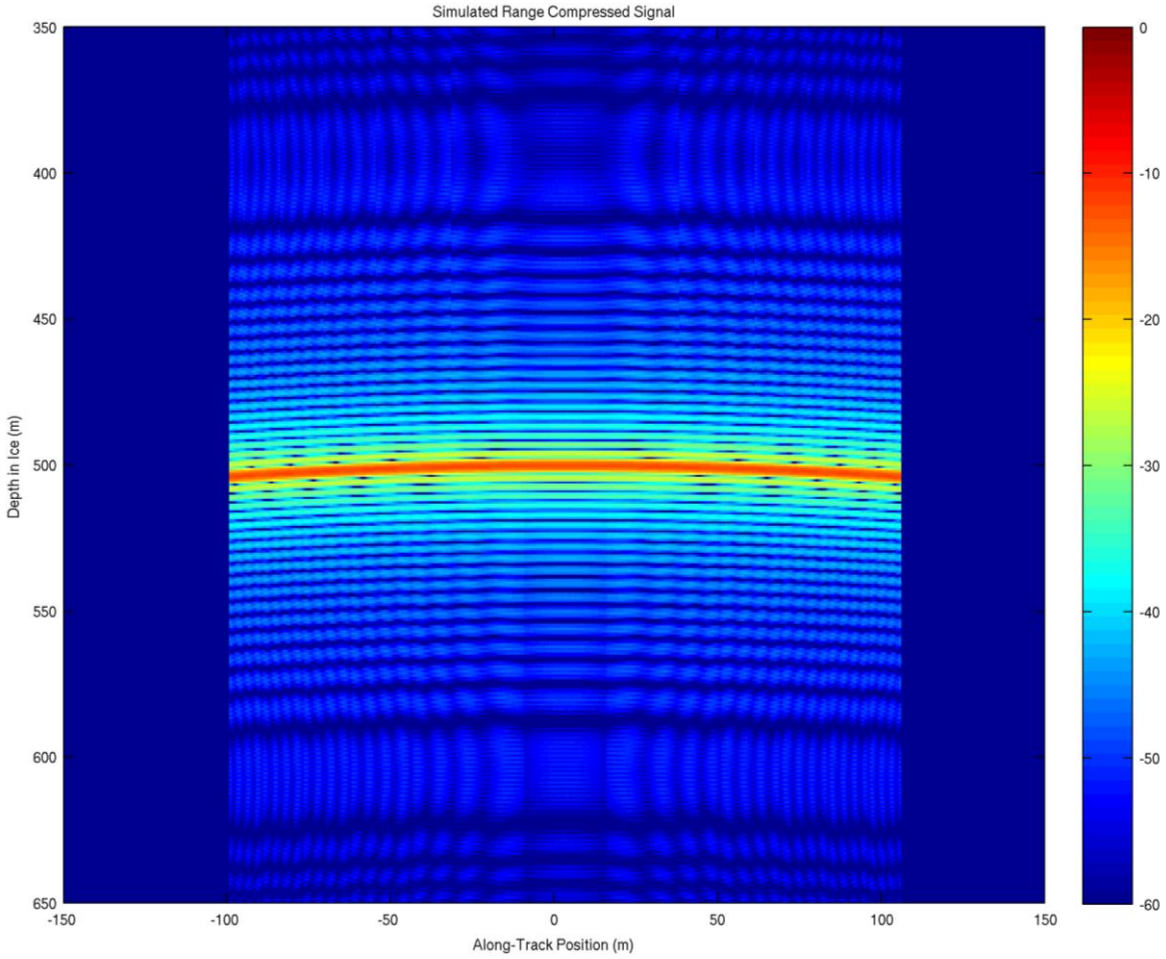

Figure 3-3: Simulated range compressed data. The color axis is relative power in dB.

3.4.3. Motion Compensation

The f-k migration and array processing algorithms require all the receivers to follow a flat, linear trajectory over the extent of the SAR aperture. This means any change in the platform's elevation, roll, pitch, or heading will cause the SNR of the processed signal to be lower than its potential. To correct this we need high precision GPS and INS data, which are typically available.

3.4.3.1. Along-Track Sample Spacing

Variations in platform velocity cause the spacing between data samples in the along-track to be non-uniformly distributed. We want the along-track sampling to be uniform and to have a specific spacing, σ_x. The choice of σ_x is discussed further in section 5.1. To achieve uniform sample spacing an output along-track vector is created and the data is fit to that spacing in the motion compensation algorithm using a sinc interpolation method.

3.4.3.2. Coordinate Systems

The motion compensation process is comprised of several steps. First the GPS and INS information must be updated with the antenna lever arm positions. Looping through each

element of the GPS/INS vector, the lever arm positions, which start in the BCS (a coordinate system which has the trajectory data as the origin), are:

1. Transformed from BCS to a vehicle-carried North-East-Down (NED) reference frame with the origin as the reference trajectory data still.
2. Transformed from a North-East-Down (NED) reference frame to the Earth-Centered Earth-Fixed (ECEF) coordinate system.
3. Transformed to geodetic coordinates using the WGS-84 ellipsoid.

For each output position of the SAR processing, a flight coordinate system (FCS) is fitted to the trajectory. The origin of the FCS for a particular position is the reference position of the array which is usually near the center of the array. The fitting process uses the part of the trajectory that contributes to that output position. However, an approximation is made that the SAR aperture is fixed so that only one output position and FCS is needed per output range line (i.e. even though the output phase center actually varies with range, only one output phase center is recorded). In summary, for each output position, there is a unique FCS and each element of the array is written in terms of this FCS. This is required for the array processing step and allows complex geometries for the SAR flight line including circular flight paths. See Figure 3-4 for a graphical representation and appendix E for more on coordinate systems.

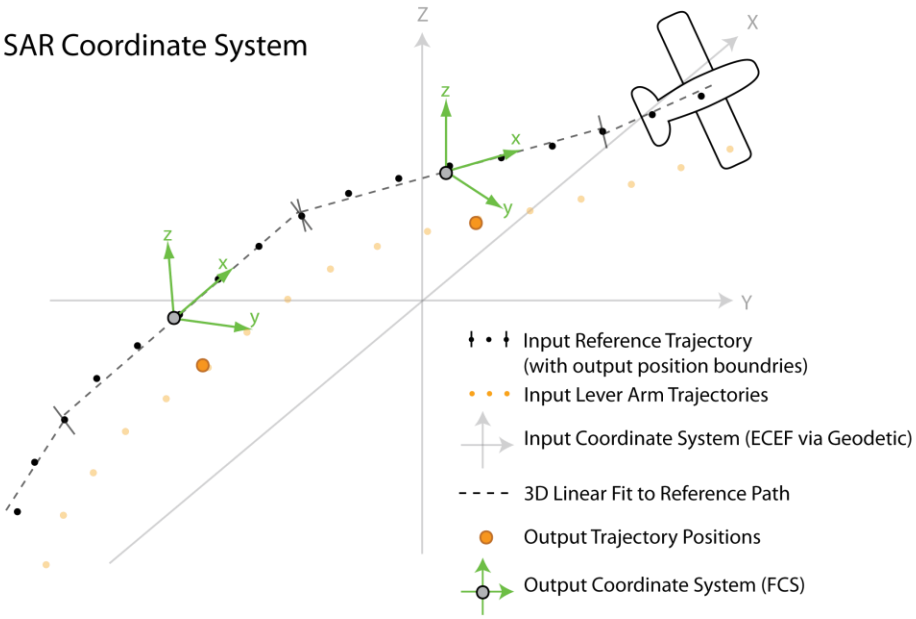

Figure 3-4: SAR coordinate system.

The squint angle for SAR processing refers to the look angle of the center of the Doppler bandwidth used for processing. In our case the squint angle is nadir or directly in the negative-z direction in the FCS and can be described by the vector

$$\theta_{squint}(x, y, z) = (0,0,-1). \tag{33}$$

The motion compensation routine takes each reference position and fits a line to the reference trajectory associated with the input used to generate that output – again using the assumption of a fixed SAR aperture length to determine the contributing input points. Once the fitted line has been determined for that output, the input positions nearest to that output are motion compensated to this fitted line. Let $\overrightarrow{r_{offset}}$ be the offset between the actual position and the fitted line. The motion compensation is broken into two steps. The first step exactly compensates the offset in along-track by adjusting the along-track position for the particular element to properly account for this offset (during uniform interpolation these adjusted along-track positions are used). The second step corrects for range errors in the squint direction for the part of the offset perpendicular to the along-track or

$$\Delta r = \langle \theta_{squint}, \overrightarrow{r_{offset\perp \vec{x}}} \rangle. \tag{34}$$

The range corrections are applied to the data as a time shift which is done as phase shifts in the frequency domain or $e^{j2\pi f_n\left(\frac{-2\Delta r}{c}\right)}$ for each frequency f_n.

The final motion compensation step is to uniformly sample the input data at the spacing of the desired output positions. A sinc kernel is used which allows the interpolator to simultaneously low pass filter the data. A modulated sinc kernel is needed to handle squint angles with a non-zero center frequency for the Doppler (i.e. so the data are band-passed filtered rather than low pass filtered).

3.4.4. Azimuth Compression via F-K Migration

As the radar travels over the target the reflected energy is spread over a hyperbola in the along-track dimension as seen in Figure 3-3. To collapse this energy back to the target location we must use some type of SAR processing algorithm. The frequency-wavenumber (f-k) migration algorithm is a computationally efficient method which makes it advantageous for large quantities of data. The main drawbacks of f-k migration are its requirement of a perfectly straight trajectory over the SAR aperture length and uniform sampling of data in the along-track dimension.

A signal's wavenumber is defined as $k = \frac{4\pi}{\lambda} = \sqrt{k_x^2 + k_y^2 + k_z^2}$ and describes its spatial frequency component. In our case k_y is assumed to be zero.

F-k migration uses a 2-D FFT to transform the data from the position-time (x-t) domain to the frequency-wavenumber domain. In the f-k domain each pixel of the data is a plane wave component of the signal's frequency response with a certain wavenumber in the along-track dimension. The data begins at time zero and each plane wave is shifted to each of the desired z-positions in the output range line. At each step the data are summed across the frequency

dimension to find the time zero-component for each plane wave and the space-domain transformed result becomes the corresponding depth row in the migrated data set.

The effect of azimuth compression is, in essence, a matched filtering technique and the expected SNR gain can be calculated using the matched filter theory we have developed. The signal in question is comprised of the elements along the hyperbola that results from range compression. The steering vector in this case can be thought of as pointing in the nadir direction.

3.4.4.1. Simulation Expectations and Results

Azimuth compression SNR gain is determined by the number of records in the SAR aperture, N_x, which is determined by the SAR aperture length, L_{sar}, and along-track resolution, σ_x. The SAR aperture length for the desired along-track resolution can be calculated using

$$L(\sigma_x) = 2z_0 \tan\left(\sin^{-1}\left(\frac{n_{ice}}{n_0}\tan^{-1}\left(\frac{\lambda}{4\sigma_x}\right)\right)\right). \tag{35}$$

Then the number of records is

$$N_x = \frac{L(\sigma_x)}{\Delta_{x,input}}. \tag{36}$$

As in range compression we consider the noise to be IID Gaussian noise. The SNR is

$$\widehat{SNR} = N_x|\boldsymbol{g}|^2\frac{|\hat{s}|^2}{\sigma_N^2}, \tag{37}$$

and assuming the elements of $\boldsymbol{g}$ are uniform magnitude (boxcar along-track beam), the SNR gain is equal to N_x.

For the simulation, we chose a SAR aperture length of 200 m. The output along-track resolution must be 3.015 m based on Equation (35).

The along-track input sampling is defined by the platform velocity, pulse repetition frequency, and hardware presums as

$$\Delta_{x,input} = \frac{v \cdot presums}{f_{PRF}} = .32\ m, \tag{38}$$

where v is the platform velocity, $presums$ is the number of hardware presums, f_{PRF} is the pulse repetition frequency.

Then the number of along-track records is $N_x = \frac{200}{.32} = 625$ records and the SNR gain is $SNR_{gain} = 27.96$ dB.

The total expected SNR is $\widehat{SNR}_{ac} = SNR_{rc} + SNR_{gain} = 81.11 + 27.96 = 109.07$ dB.

The actual SNR gain was 27.77 dB due to some truncation of the along-track distance vector in CSARP. The achieved total SNR is 109.03 dB as shown in Figure 3-6.

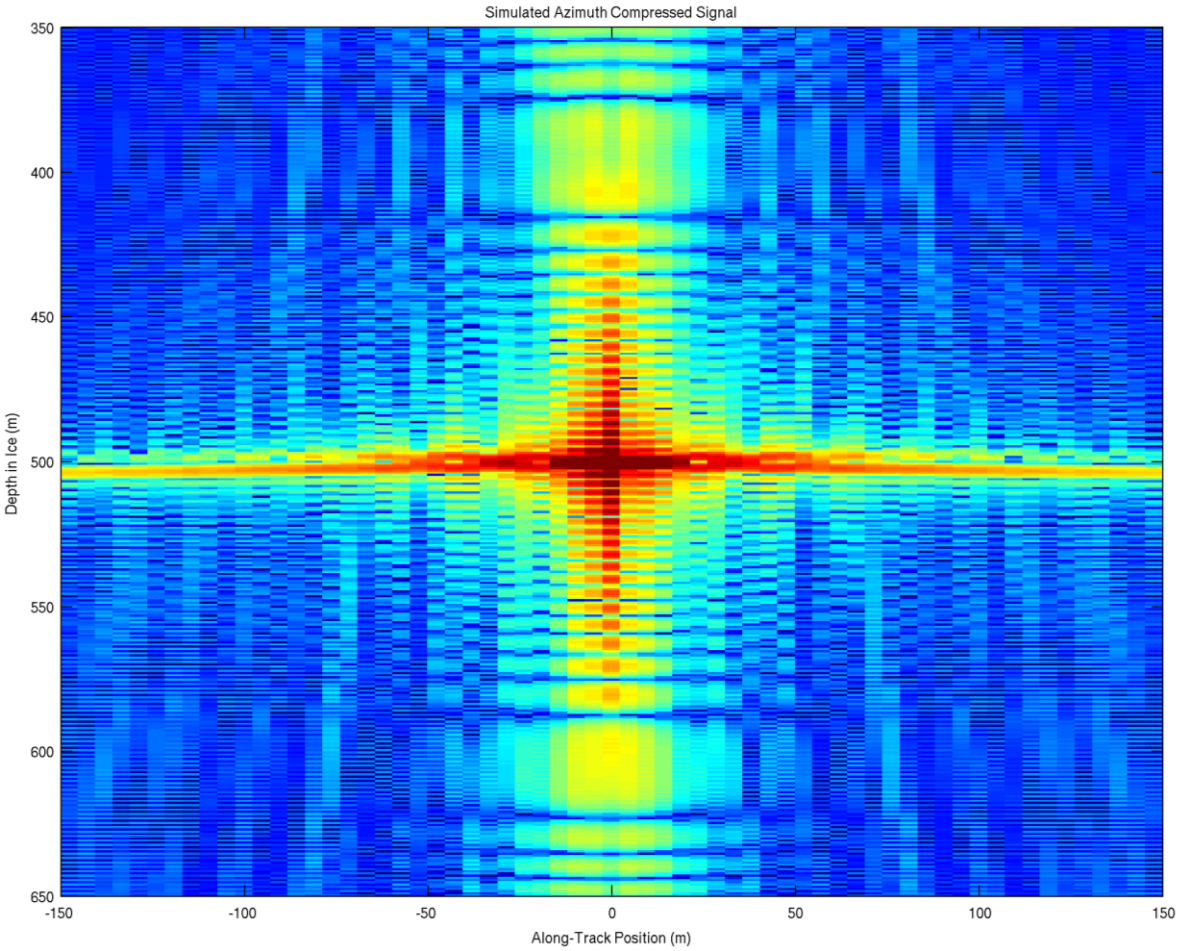

Figure 3-5: Simulated azimuth compressed data.

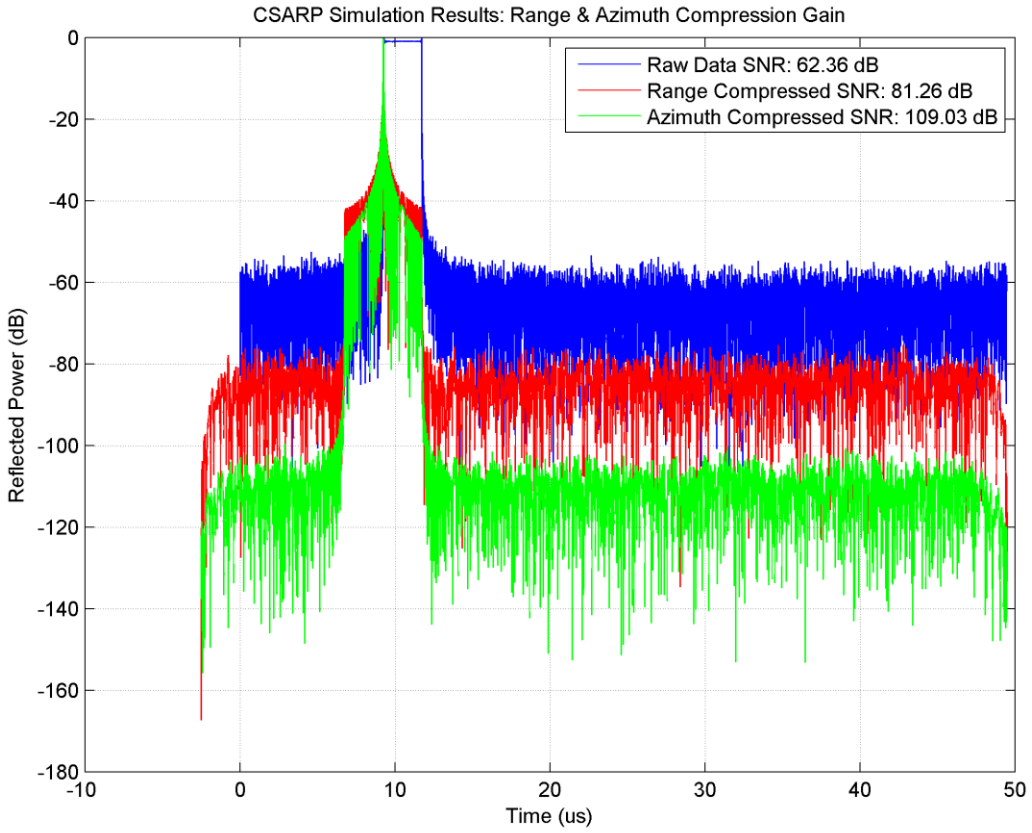

Figure 3-6: Ideal case processing gains.

3.4.5. Array Processing

In the cross-track dimension the antenna array can be combined coherently to increase the SNR of the data product. This is the same matched filtering process as the range and azimuth dimensions but noise power is no longer guaranteed to be homogeneous across all channels. The matched filtering weights in this case are:

$$\boldsymbol{w} = \frac{\boldsymbol{C}^{-1}\boldsymbol{g}}{\boldsymbol{g}^{H}\boldsymbol{C}^{-1}\boldsymbol{g}} \tag{39}$$

The expected SNR gain using these weights is:

$$\widehat{SNR} = \boldsymbol{g}^{H}\boldsymbol{C}^{-1}\boldsymbol{g}|\hat{s}|^{2} \tag{40}$$

Simulated data sets with matched and mismatched noise floors were created to test the ability of CSARP to handle this case. For imbalanced noise floors, the relative noise power added to each channel is [0 1 2 3] dB. The signal power for each channel is the same and since we are only interested in the relative change in SNR the signal power is assumed to be 1 W per channel for simplification of calculation. Since we are focused directly at nadir, $\boldsymbol{g} = [1\ 1\ 1\ 1]^{T}$. The three scenarios we are interested in are:

1) equally combining balanced noise floors,

$$\boldsymbol{C}_{eq}^{-1} = \frac{1}{\sigma_N}\boldsymbol{I_4}$$

$$\widehat{SNR}_{eq} = \boldsymbol{g}^H\boldsymbol{C}_{\boldsymbol{eq}}^{-1}\boldsymbol{g} = 6.02\ dB$$

$$\widehat{SNR} = 6.02 + SNR_{single}(dB)$$

2) matched filter combining non-homogeneous noise floors, and

$$\boldsymbol{C}_{uneq}^{-1} = \begin{bmatrix} 1 & 0 & 0 & 0 \\ 0 & 0.6310 & 0 & 0 \\ 0 & 0 & 0.3981 & 0 \\ 0 & 0 & 0 & 0.2512 \end{bmatrix}$$

$$SNR_{MF} = \boldsymbol{g}^H\boldsymbol{C}_{uneq}^{-1}\boldsymbol{g} = 3.58\ dB$$

$$\widehat{SNR} = 3.58 + SNR_{single}(dB)$$

3) equally combining non-homogeneous noise floors

$$\widehat{SNR}_{mismatch} = \frac{\left(\boldsymbol{g}^H\boldsymbol{C}_{eq}^{-1}\boldsymbol{g}\right)^{\mathbf{2}}}{\boldsymbol{g}^H\boldsymbol{C}_{eq}^{-1}\boldsymbol{C}_{uneq}\boldsymbol{C}_{eq}^{-1}\boldsymbol{g}} = 2.46\ dB$$

$$\widehat{SNR} = 2.46 + SNR_{single}(dB)$$

Figure 3-7 shows the simulation results for each case. In this case we achieved over 1 dB improvement in SNR over four channels by using the matched filter.

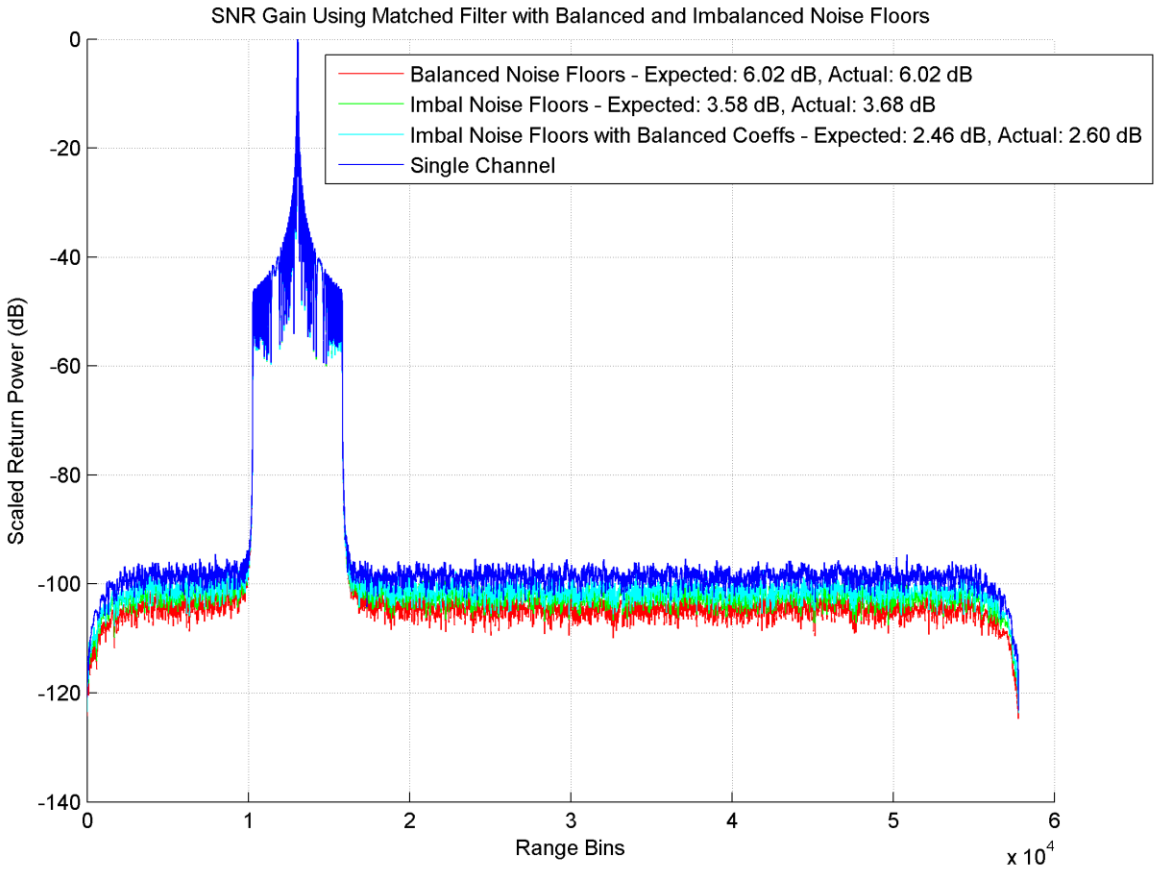

Figure 3-7: SNR gain due to matched filtering based on individual channel noise power.

3.5. **Lever Arm Verification**

As discussed in section 2.2.2 the antenna lever arm is the displacement between the measurement phase center and the trajectory reference point. The lever arm is needed to determine the exact position of a measurement. If the lever arm is not properly compensated for, a signal received by multiple antennas will contain time delay mismatches and, when combined, will produce sub-optimal results. To verify the lever arm is properly compensated for, a simulated data set with four antenna elements was created with no lever arm information (i.e. all data collected as though at the trajectory reference point). Then the data were processed normally (i.e. with a non-zero lever arm). The time delay offset, and subsequent drop in SNR, caused by this mismatch in lever arms is calculated and compared to the results after processing.

The ideal phase offsets are

$$\boldsymbol{\theta}_{ideal} = [0, 0, 0, 0]°.$$

If the channels were aligned properly, the expected SNR gain of the combination would be

$$SNR_{ideal} = \sum e^{j(\theta_{ideal} - \theta_{ideal})} = 6.02\ dB.$$

In other words, that of coherent integration of four records with phase matched signal and uncorrelated white noise.

However, if not aligned, the SNR gain will be slightly less due to the phase mismatch. With a simulation trajectory with zero roll, the extra range for each element for our particular setup is

$$[0.578, 0.568, 0.558, 0.549] \text{ m.}$$

At the center frequency $f_c = 195\ MHz$ the phase offset is

$$\boldsymbol{\theta}_{mismatch} = [270.57, 266.03, 261.49, 256.95]°.$$

The corresponding SNR is:

$$SNR_{mismatch} = \sum e^{j(\theta_{mismatch} - \theta_{ideal})} = 5.97\ dB.$$

The SNR loss is 0.05 dB. Larger lever arm differences would result in more loss of SNR. Although the loss in SNR is negligible for this example when considering regular beam forming, proper data collection positions are critical for clutter suppression techniques such as MVDR or the MUSIC algorithm.

Figure 3-8 verifies the phase offset between channel one and each other channel when the lever arm is applied in processing but not present in data simulation. Figure 3-9 shows the expected SNR is achieved when the lever arm is applied properly, 6.02 dB expected vs 6.11 dB actual, and when the lever arm is not applied, 5.97 dB expected vs 5.85 actual. The difference of .1 dB between expected and actual is due to the statistical nature of the noise.

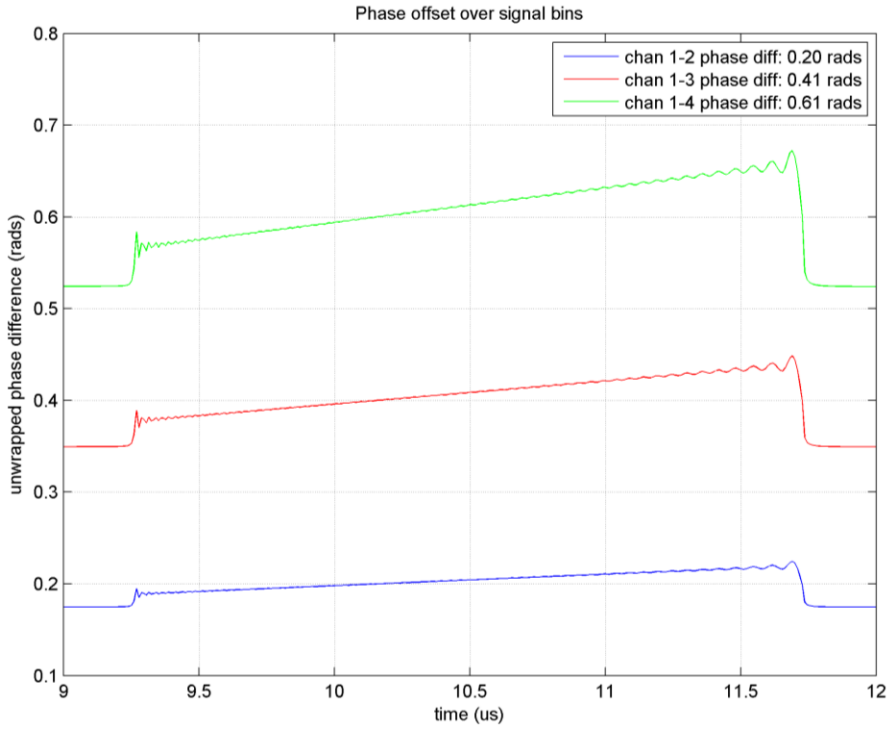

Figure 3-8: Phase offset caused by antenna lever arm.

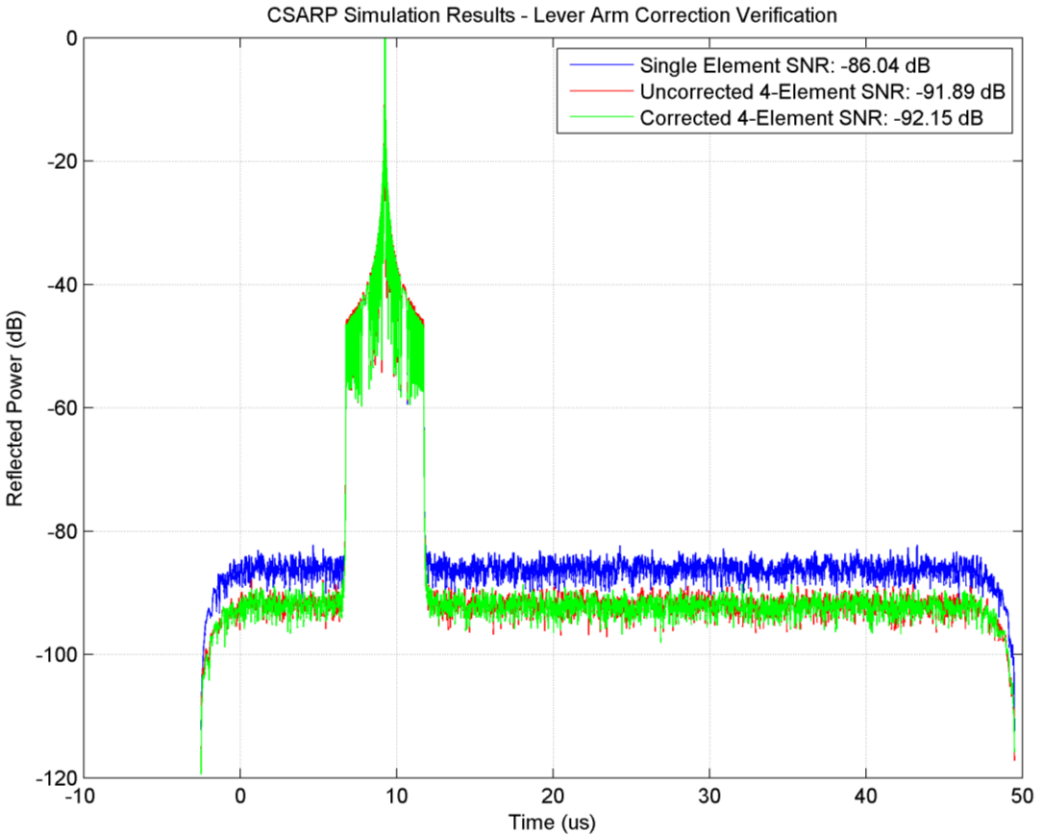

Figure 3-9: Array gain with and without lever arm included.

3.6. SNR Measurement Method

SNR is the primary metric of interest in all tests in this thesis. The SNR of the data is measured between the peak power of the target response and the average power of the noise floor. To avoid having to do multiple simulation runs to acquire an accurate SNR estimate, we use a large SNR for the baseline. Also, the typical processing is done at the Nyquist sampling frequency for efficiency and this must be compensated for when measuring the peak value since the sampling may not line up with the peak. We want to increase the sampling rate of the signal to get a more accurate value for the target peak power. Zero padding in the frequency domain interpolates between samples in the time domain as shown in Figure 3-10.

For raw data, where there is no single peak, the SNR is calculated analytically based on the values used in the simulator. Because the simulated data has only one target it is also interpolated to a higher number of samples in the along-track dimension to more precisely detect the peak target response. For real data the peak signal power is calculated as the incoherent average power of the target response from a large number of data records. The average noise power in both cases is taken from the incoherent average of a large number of data records in the ranges after all signal returns but before the attenuating effect at the end of each record due to correlation in the range compression step. The A-scopes (single receive records) under comparison are translated so the peak target return has a value of zero dB then the SNR is simply the average noise power negated, as shown in Figure 3-6.

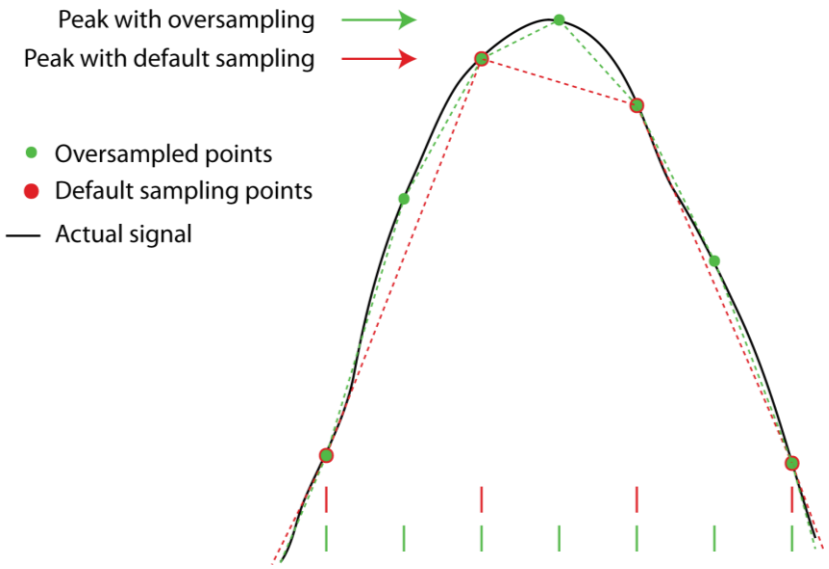

Figure 3-10: Interpolation for improved resolution of higher frequency details.

4. CHANNEL EQUALIZATION

Many array processing algorithms require the timing and amplitude of all receivers to be precisely matched. There are a number of elements in the receive chain that add both linear and non-linear time, phase, and amplitude errors to the signal recorded on each element. Since it is difficult to measure these properties in the components themselves, a data-dependent approach is used to quantify the errors, or mismatches, caused by them.

4.1. Calculating Channel Equalization Coefficients

Equalization coefficients are calculated for the signal recorded on each channel, $s(t)$, with respect to a reference channel, $s_{ref}(t)$. A channel equalization coefficient is comprised of a time delay, amplitude, and phase component. The time delay correction is a multi-wavelength correction while the phase correction is on the sub-wavelength level. See Figure 4-1 for a visual representation of the channel equalization coefficient components.

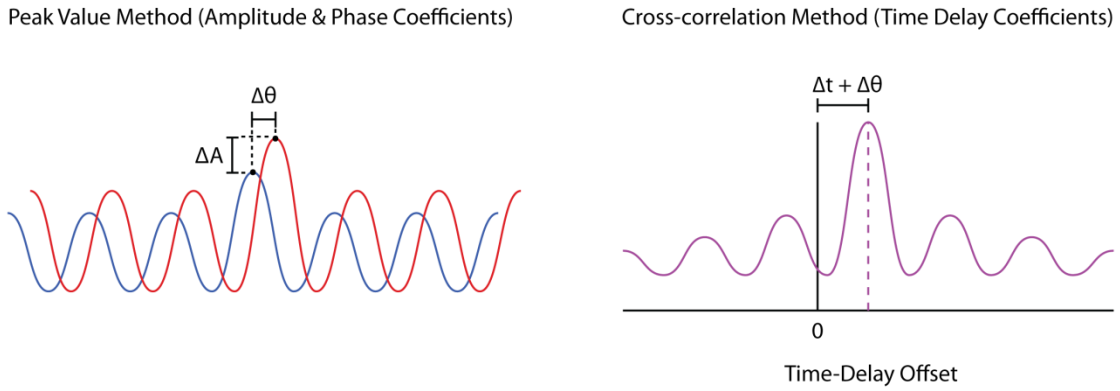

Figure 4-1: Channel Equalization Coefficient Components

Before the data are analyzed to determine equalization coefficients, some pre-conditioning steps are applied. First, the data are motion compensated for attitude and array position to remove any lever arm effects. Next, a basic surface layer tracker is used to locate the desired target, the nadir surface reflection, for creating coefficients. The signal and noise power are calculated for each record of the data, then the data are culled to reject any records with a SNR below a certain threshold. Finally, time delay, phase, and amplitude corrections are calculated.

Since the time-delay correction also affects the phase, the time-delay correction is determined first and then applied to the data before the phase correction is found. The method used for determining the time delay correction is taking the cross-correlation of the reference channel and the active channel and determining the peak offset as follows:

$$s_k = \sum_{j=0}^{N} s_{ref}^{*}[j]\, s[j+k]. \tag{41}$$

If the signals are perfectly aligned in time, the peak, s_{peak}, of the result will appear at the center time value. The cross-correlated result is over-interpolated by an interpolation factor of M,

$$s_n = \sum_{k=0}^{N-1} S_k e^{j\frac{2\pi kn}{MN}} \;\; \forall n = 0 \ldots MN-1, \tag{42}$$

where

$S_k =$ Frequency domain signal component of s_k,
using a frequency domain interpolation method to provide a more precise time delay value. An oversampling value of M = 100 is usually used. The offset between $s_{peak} = \max(s_{interp})$ and the zero time value of the interpolated signal, $s_{interp}(0)$, is the required time delay correction, $\Delta t = s_{peak} - s_{interp}(0)$.

The reference channel is typically one that is connected to an antenna in the center of the array to minimize the average distance between all channels. Minimizing the average distance should minimize the decorrelation of the signals received by two receivers so that the cross-correlation method used to calculate the time delay will be more accurate. To determine the phase and amplitude coefficients we use a signal peak comparison method where the same range bin is used in each record to compare the phase and amplitude. Fourier interpolation is also applied here. This should only be done after the time delay correction has been calculated and applied to the data. This method identifies the peak value and corresponding range bin for the reference signal, $s_{ref}(t)$ and the value of the active signal, $s(t)$ at the same range bin, and the difference between their phase and amplitude values are the phase and amplitude equalization coefficients.

Although motion compensation is applied before calculating the coefficients, data with small roll angles tends to work better than data with large roll angles. Since most of the operational data are collected at small roll angles it makes sense to use similar data to generated the equalization coefficients. The difficulty of working with large roll angles is probably due to the increased probability that the peak searching routine incorrectly identifies off nadir returns but may also be due to imperfections in our understanding of the steering vector or motion compensation.

4.2. **Applying Equalization Coefficients**

The application of equalization coefficients in the simulator is covered in section 2.3.3. The application in CSARP is very similar but is applied in different stages. The time delay coefficients are applied to the reference pulse,

$$s_{ref}[n] = \frac{1}{N}\sum_{k=0}^{N-1} S_{ref,f}[k]\, e^{-j\frac{2\pi k f EQ_{td}}{N}} e^{-\frac{j2\pi kn}{N}},$$

where

$S_{ref,f}[k]$ is the discrete frequency transform of $s_{ref}[n]$,

while the amplitude and phase coefficients are applied to the recorded data through a simple multiplication

$$x[n] = EQ_{chan} \cdot x[n],$$

where

$EQ_{chan} = 10^{\frac{EQ_{amp}}{20}} e^{jEQ_{\phi}\frac{\pi}{180}}$,

EQ_{td} are the time delay mismatches in seconds,

EQ_{amp} are the power mismatches in dB,

EQ_{ϕ} are the phase mismatches in degrees,

$x[n]$ is the recorded radar signal.

4.3. **Targets**

Ocean data are ideal for channel equalization for several reasons. First of all, because it is a specular target with a very high dielectric contrast at the interface ($\epsilon_{air} = 1, \epsilon_{water} = \sim 80$ [6]) much of the signal energy is reflected back to the radar giving the recorded signal a very high SNR. In fact, it has such a strong reflection that the recorded signal will be saturated when all transmitters are used over the ocean. Secondly, the first return from the ocean surface is usually limited to small angles around nadir and this return is generally dominant since it is flat on a large-scale. This is in contrast to the response from a rough bed which will often have a peak at off-nadir angles and the radar echo return will fall off more slowly at larger angles. The worst clutter typically occurs along outlet glaciers when the range to the exposed bedrock at the edge of the glacier occurs at the same range, but different angle, as the target of interest. The reflection from both features arrive at the radar at close to the same time and the unwanted returns from the exposed sides make the target return difficult to distinguish (see Figure 4-2). This would make it difficult to obtain a clean phase and amplitude from the target used for channel equalization. A field season should include several segments with calibration data taken over the ocean from a high altitude.

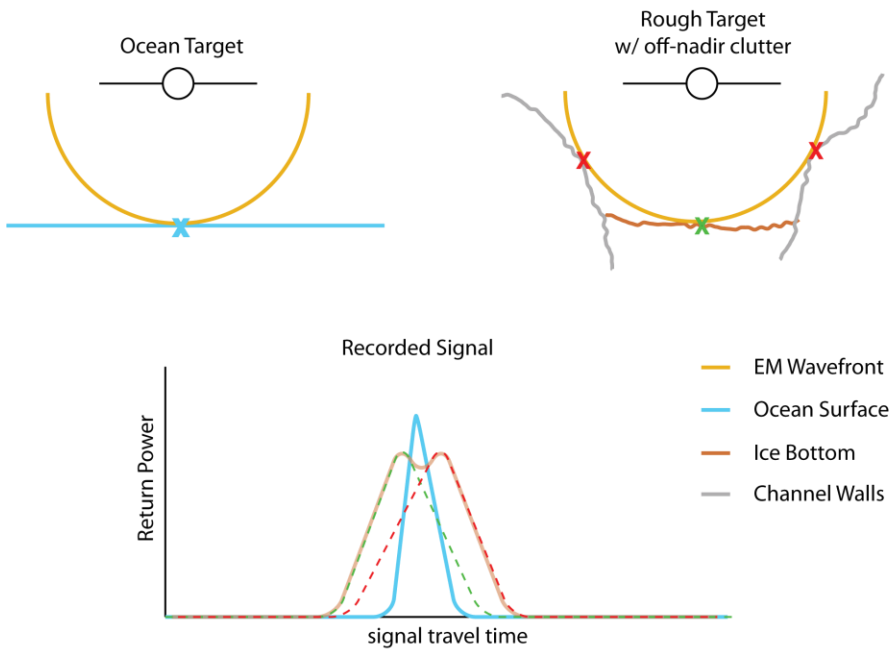

Figure 4-2: Simple diagram showing the single return from ocean data and an example of ambiguous returns from an outlet glacier channel.

4.4. 2011_Greenland_P3 Mission Specs

The data used for validating the equalization code is from the 2011 mission to Greenland aboard the NASA P-3 Orion aircraft. The P-3 is a four-engine turboprop with a flight range of 8-12 hours at up to 330 knots. CReSIS mounted 15 broadband dipole antennas on the aircraft, 7 below the fuselage and 4 on each wing. The signal was transmitted from the center 7 elements and recorded on all 15, usually alternating between a 1 us and 10 us pulse chirped pulse with a .2 Tukey taper applied. More radar parameters are available in Table 4-1.

Table 4-1: 2011 Greenland P3 Radar Parameters [5]

Radar Carrier Frequency	195 MHz
Signal Bandwidth	30 MHz
Peak Transmit Power	57 dBm
Transmit Pulse Duration	1 to 30 μs
Pulse Repetition Frequency	~12 kHz programmable
Transmit Tukey Taper	0.2
Antenna Type	Planar dipole array: 7-elem Tx/Rx array two 4-element Rx array
Antenna Gain	Tx array: 15.5 dBi and Single Rx: 7 dBi
Cross Track Beamwidth	17°
Radar Pulse-Limited Footprint	420m
A/D Dynamic Range	14-bits
Receiver Noise Figure	4 dB
Sampling Frequency	111 MHz

4.5. **Equalization Outputs**

When the equalization code has finished running there are four main outputs. One is the final equalization coefficients and their difference from the initial coefficients that can be seen in Table 4-3, Table 4-4, and Table 4-5 below. The other three are plots of the final index, phase, and power offsets for each of the channels. Figure 4-3, Figure 4-4, and Figure 4-5 below show the final index, phase, and power offsets for the reference data set both before and after equalization. Results after equalization are not expected to be perfectly compensated because the coefficients are calculated as the average over a large number of records.

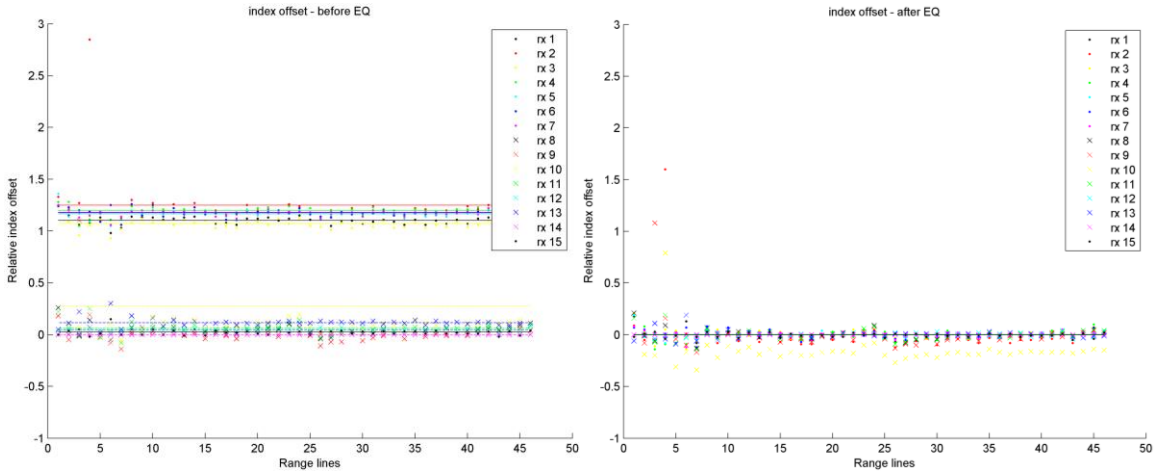

Figure 4-3: Plot of index offsets before (left) and after (right) equalization for the reference data set.

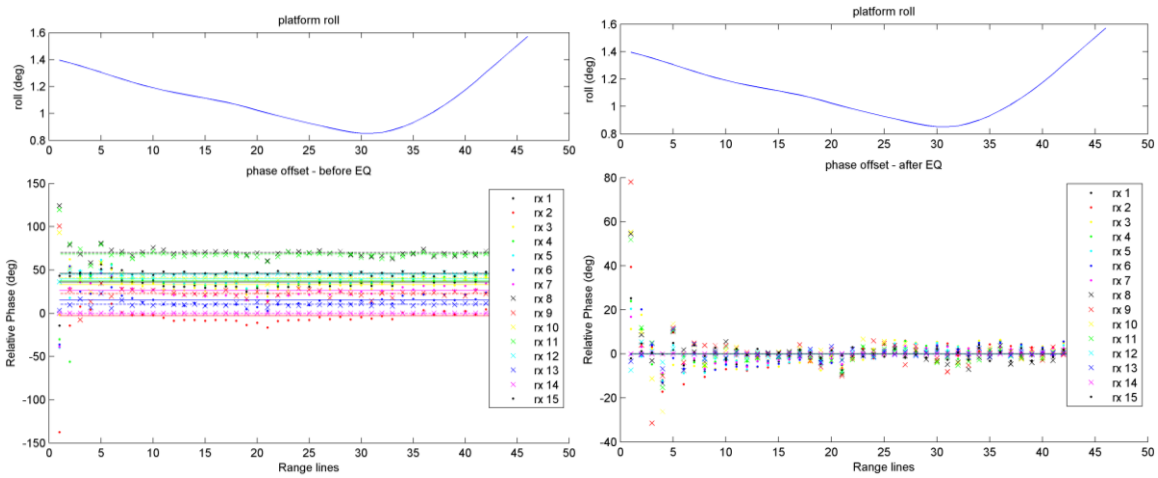

Figure 4-4: Plot of phase offsets before (left) and after (right) equalization for the reference data set.

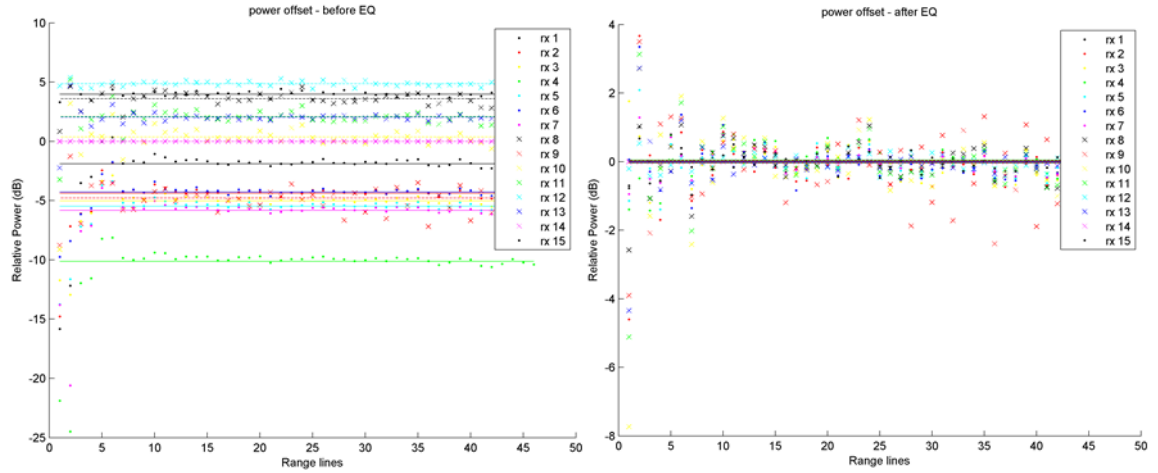

Figure 4-5: Plot of power offsets before (left) and after (right) equalization for the reference data set.

4.6. Expected SNR Gain

The expected SNR gain is comprised of the gain resulting from equalizing the channels to bring their phase and amplitude into alignment and from the combination of the channels based on their noise power via matched filtering.

4.6.1. Expected Equalization Gain

The expected SNR gain from channel equalization can be calculated from the channel equalization coefficients. We ignore the time delay coefficients, which are only used to get the signal envelopes to align. Since our goal is for the array to be phase matched and have uniform amplitude the expected gain is simply the power of phase and amplitude corrections. The complex coefficients,

$$EQ_{cplx}(chan) = 10^{\frac{EQ_{amp}(chan)}{20}} \cdot e^{-jEQ_{\phi}(chan)\frac{\pi}{180}}, \tag{43}$$

when applied result in signal power of,

$$P = \left(EQ_{cplx} \cdot Ae^{j\phi}\right)^* \cdot \left(EQ_{cplx} \cdot Ae^{j\phi}\right) = Ae^{-j\phi} \cdot W \cdot Ae^{j\phi}$$

$$W = \begin{bmatrix} EQ_{cplx,1} & \cdots & 0 \\ \vdots & \ddots & \vdots \\ 0 & \cdots & EQ_{cplx,N} \end{bmatrix}$$

$$P_S = \sum_{i=1}^{N} \left|EQ_{cplx,i}\right|^2 A_i^2$$

Prior to equalization the relative signal power of the combined channels can be found by summing the amplitude error coefficients,

$$P_{S,1} = \sum_{i=1}^{N} \left|10^{\frac{EQ_{amp,i}}{20}}\right|^2. \tag{44}$$

This signal power is relative to the reference channel. The amplitude and phase coefficients are combined to create complex coefficients

The expected relative signal power of the combined channels after equalization is the sum of the complex coefficients,

$$P_{S,2} = EQ_{cplx}^* \cdot EQ_{cplx}. \tag{45}$$

The ratio of these two power values, $\frac{P_{S,1}}{P_{S,2}}$, gives the increase in signal power due to the phase correction. We have assumed here that the noise is white Gaussian so that the phase correction will not change the noise from element to element. The amplitude correction will change the noise power of each channel relative to the reference channel so the total relative noise power will increase by the average of the amplitude equalization coefficients,

$$\frac{1}{N}\sum_{i=1}^{N} EQ_{amp,i}. \tag{46}$$

4.6.2. Matched Filter Gain

If the calculated coefficients are optimal then the signal amplitude and phase will be matched across the channels but there may still be a mismatch in the noise power due to slight differences in the components of the receive chain for each element. This mismatch is best dealt with using a matched filter in the across-track dimension. The matched filter keeps any signal with higher noise power from dominating the combined results.

The expected matched filter gain, based on the noise covariance matrix, is calculated using equations (25), (26) and (27) from section 3.3.2. Channel equalization coefficients should be applied before calculating the noise covariance matrix as the amplitude coefficients will affect the noise power.

4.6.3. Channel Equalization Simulation Parameters

To verify that the channel equalization coefficients are properly applied in CSARP, a set of arbitrary coefficients are added during data simulation then removed in CSARP.

Table 4-2: Channel Equalization Simulation Parameters

Parameter	Symbol	Value
Time delay errors	EQ_{td}	[0 2 4 6] ns
Phase errors	EQ_{ϕ}	[0 10 20 30] °
Amplitude errors	EQ_{amp}	[0 1 2 3] dB

Using channel one as the reference channel, the expected signal power for uniform weighting is given by equation (44),

$$P_{S,1} = 5.84 \quad or \quad 7.66\ dB,$$

the unequal signal power is given by equation (45),

$$P_{S,2} = 4.39 \quad or \quad 6.43\ dB,$$

and the expected gain is given by the ratio,

$$\frac{P_{S,1}}{P_{S,2}} = 1.19 \quad or \quad 0.76\ dB.$$

4.7. Reference Data

There are two high-altitude over ocean data sets for the 2011_Greenland_P3 season. These datasets were collected with a single element transmit waveform pattern so that these segments do not have a saturated return signal. The transmit calibration waveform schedule uses each transmit element separately, thus reducing the transmitted power by a factor of seven and received power by a factor of seven squared, due to the loss of the transmit antenna gain too. The coefficients retrieved from this data are shown in Table 4-3, Table 4-4, and Table 4-5. These coefficients are used as the reference for coefficient verification using different targets.

Table 4-3: Time Delays for Reference Data

	Time Delay (ns)														
Day_Segment	1	2	3	4	5	6	7	8	9	10	11	12	13	14	15
20110409_08_31	1.9	5.8	0	5.6	3.4	4.1	4	-32.8	-36.6	-26	-30.7	-33.2	-28.7	-35.1	-33.9
20110409_08_33	2.8	6.7	0	5.7	3.7	4.3	4.1	-31.8	-31.6	-30.1	-26.7	-34.1	-28.9	-32.2	-27.2
20110409_08_34	2.6	6.3	0	6.1	3.5	4.3	4.3	-29.8	-34	-31.1	-32.7	-38.6	-35.2	-38.5	-39.7
20110409_08_35	2.1	5.3	0	5.9	3.2	4.4	3.9	-33.9	-33.6	-31.9	-32.4	-33.1	-31.9	-33.1	-34.9
20110409_08_36	1.6	5.1	0	5.6	3.3	4.2	4.1	-33.7	-35.4	-31.9	-33.4	-32.8	-30.7	-34.6	-34.1
20110409_08_37	1.7	4.9	0	5.5	3.1	4.1	3.5	-34.2	-35	-32.3	-33.3	-33.6	-31.7	-34.8	-34.6
Ref	2.1	5.7	0	5.7	3.4	4.3	4	-32.7	-34.4	-30.5	-31.5	-34.2	-31.2	-34.7	-34.1

Table 4-4: Amplitude Offsets for Reference Data

	Amplitude Offsets (dB)														
Day_Segment	1	2	3	4	5	6	7	8	9	10	11	12	13	14	15
20110409_08_31	3.3	1.7	0	-4.4	0.3	1.5	0	2.9	-5.4	-0.2	1.4	4.2	1.5	-0.6	3.3
20110409_08_33	3.4	1.8	0	-4.3	0.4	1.5	-0.1	3.5	-5.1	0.2	1.9	4	1.2	-0.9	2.9
20110409_08_34	3.4	1.8	0	-4.3	0.4	1.6	0.3	3	-5.5	-0.3	1.4	4.6	1.9	0.1	3.8
20110409_08_35	3.2	1.5	0	-4.3	0.1	1.5	0	2.6	-5.3	-0.5	1.4	4.2	1	-0.4	3.2
20110409_08_36	3.2	1.6	0	-4.1	0.3	1.5	0	2.9	-5.6	-0.4	1.3	4.5	1.6	-0.4	3.6
20110409_08_37	3.1	1.4	0	-4.1	0.1	1.4	-0.1	2.6	-5.4	-0.6	1.2	4.2	1.1	-0.7	3.3
Ref	3.3	1.6	0	-4.3	0.3	1.5	0	2.9	-5.4	-0.3	1.4	4.3	1.4	-0.5	3.4

Table 4-5: Phase Offsets for Reference Data

	Phase Offsets (degrees)														
Day_Segment	1	2	3	4	5	6	7	8	9	10	11	12	13	14	15
20110409_08_31	1.8	-37.1	0	9.2	6	-20.3	-8.7	-95.3	98.3	29.6	-13.2	134.6	-50	54.8	142.6
20110409_08_33	2.3	-36	0	9.1	6.7	-18.8	-8.2	-99.2	94.7	26.8	-17.2	138.9	-45.2	57.5	145.3
20110409_08_34	2.3	-34.7	0	8.5	7.2	-19	-8.1	-92.6	103.7	32.7	-10.5	135.1	-48.3	55.1	144
20110409_08_35	0.1	-36.7	0	8.9	6	-20.1	-7.1	-94.4	102.7	29.8	-8.8	135.1	-46.3	56	145.5
20110409_08_36	1.7	-37.9	0	9.6	5.7	-20.7	-9.3	-93.6	99.2	31.5	-11.6	136.9	-47.3	57	145.8
20110409_08_37	2.1	-37.2	0	13.7	6.5	-20.3	-7.8	-92.5	100.1	31.2	-10.5	140	-44.1	60.9	150.4
Ref	1.7	-36.6	0	9.8	6.4	-19.9	-8.2	-94.6	99.8	30.3	-12	136.8	-46.9	56.9	145.6

4.8. **Processing Improvement**

Table 4-6 shows a sample noise covariance matrix from the processed data set 20110502_02_024. The data set taken over the center of the ice, exhibits the cleanest internal noise spectra from this field season (Theresa Stumpf, personal communication, Nov 20th, 2012). The flatness of the ice surface in the center of the ice allows for the assumption that the section of the return record below the bedrock is free of interference other than thermal noise.

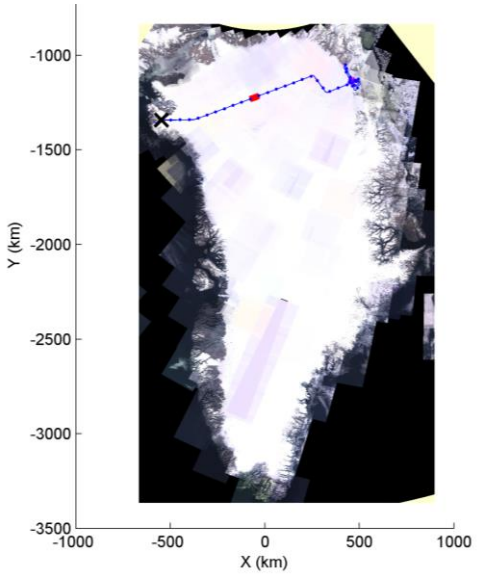

Figure 4-6: Map showing the location of the data used for the sample covariance matrix in Table 4-6.

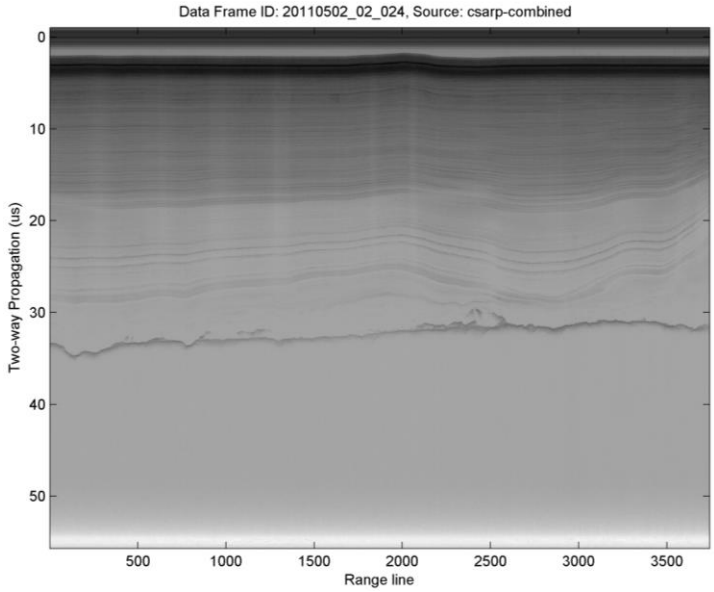

Figure 4-7: Clean noise data used for creating the covariance matrix in Table 4-6.

Table 4-6: Sample covariance matrix in dB and scaled to the channel with the lowest overall noise power (channel 12).

Chan	1	2	3	4	5	6	7	8	9	10	11	12	13	14	15
1	1.24	-7.18	-8.25	-6.63	-4.58	-5.36	-7.16	-15.8	-9.7	-15.1	-21.6	-21.4	-15.3	-16.3	-17.2
2	-7.18	1.98	-3.12	-5.93	-6.66	-6.86	-9.68	-14.8	-9.98	-15.8	-17.4	-19.4	-15.7	-15.8	-17.9
3	-8.25	-3.12	4.59	-4.9	-6.23	-8.96	-14.5	-13.8	-8.24	-13.9	-15	-25.5	-16.6	-18.1	-20
4	-6.63	-5.93	-4.9	7.01	-3.78	-6.93	-7.69	-12.8	-8.16	-12.3	-15	-17.9	-16.6	-13.6	-20.5
5	-4.58	-6.66	-6.23	-3.78	4.62	-1.07	-3.06	-15.9	-5.9	-8.97	-20.9	-15.5	-17.4	-13.4	-14.1
6	-5.36	-6.86	-8.96	-6.93	-1.07	2.5	-4.11	-17.3	-8.62	-12.6	-17.2	-21.5	-15.3	-15.6	-19.6
7	-7.16	-9.68	-14.5	-7.69	-3.06	-4.11	1.88	-18.4	-8.95	-13.9	-19	-21.2	-17.4	-17.2	-17.4
8	-15.8	-14.8	-13.8	-12.8	-15.9	-17.3	-18.4	0.89	-7.21	-13.2	-17	-26	-21.7	-20	-21.9
9	-9.7	-9.98	-8.24	-8.16	-5.9	-8.62	-8.95	-7.21	9	-5.91	-7.29	-20.8	-15.4	-16.8	-18.8
10	-15.1	-15.8	-13.9	-12.3	-8.97	-12.6	-13.9	-13.2	-5.91	4.26	-3.96	-20.3	-19.2	-16.1	-21.1
11	-21.6	-17.4	-15	-15	-20.9	-17.2	-19	-17	-7.29	-3.96	3.22	-26.4	-22.2	-23	-19.9
12	-21.4	-19.4	-25.5	-17.9	-15.5	-21.5	-21.2	-26	-20.8	-20.3	-26.4	0	-16.3	-14.2	-16.1
13	-15.3	-15.7	-16.6	-16.6	-17.4	-15.3	-17.4	-21.7	-15.4	-19.2	-22.2	-16.3	1.3	-11.3	-13.3
14	-16.3	-15.8	-18.1	-13.6	-13.4	-15.6	-17.2	-20	-16.8	-16.1	-23	-14.2	-11.3	2.63	-5.27
15	-17.2	-17.9	-20	-20.5	-14.1	-19.6	-17.4	-21.9	-18.8	-21.1	-19.9	-16.1	-13.3	-5.27	0.34

This matrix is made up of over 2,000,000 samples of noise signal. This matrix is calculated after equalization coefficients are applied and is scaled to the lowest channel noise power. In this sample, channel 12 has the lowest noise power and channel 9 has the highest (9 dB higher than channel 12.) The significantly higher noise power in channel 4 (2.35 dB higher than the next highest noise power in the center array) is likely due to the extra narrowband interference present uniquely in that channel, shown in Figure 4-8 around 196 & 200 MHz.

Also of note is the noise covariance between different channels in each array and between arrays (off-diagonal elements). Assuming white Gaussian noise there would be zero noise covariance between a particular channel and all other channels but as Table 4-6 shows there is as little as 1 dB difference between adjacent channels, possibly caused by the coherent noise common to all channels around 194 MHz.

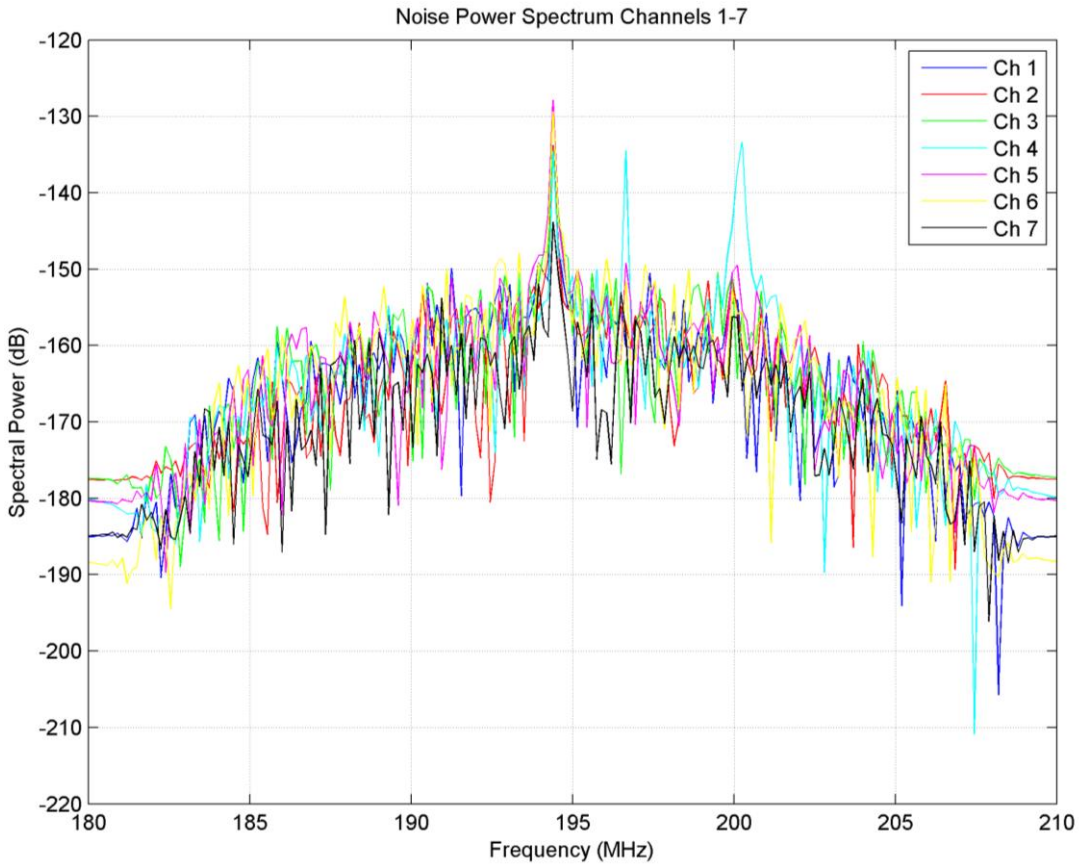

Figure 4-8: This noise power spectrum for 20110502_02_024 shows added interference for channel 4, the central channel of the center transmit/receive array.

The expected signal power due to equalization from equation (44) is

$$P_{S,1} = 56.21 \; or \; 17.50 \; dB.$$

Without equalization, the signal power is given by equation (45),

$$P_{S,2} = 41.35 \; or \; 16.16 \; dB,$$

and the expected gain from equalization is given by the ratio,

$$\widehat{SNR}_{eq} = \frac{P_{S,1}}{P_{S,2}} = 1.36 \; or \; 1.34 \; dB.$$

Both the matched (25) and mismatched (26) filter results are averaged over many sets of snapshots to create a representative expected SNR gain using equation (27)

$$\frac{P_{N-mismatched}}{P_N} = 2.46 \; dB. \tag{27}$$

4.9. **Coefficient Stability and Target Diversity**

In order to have confidence that the coefficients are only a product of differences in the receive chain we need many records where a range-isolated target at nadir is present. By averaging coefficients obtained from many records we can have confidence that the coefficients are coming from the radar system rather than the target. Table 4-3, Table 4-4, and Table 4-5 show the coefficient stability over the frames of data used for the reference coefficients. We can further build our confidence of these coefficients by comparing them to other types of targets from different times in the season and different locations. Targets with low SNR, clutter noise, or complex layering should be avoided for the purposes of determining or validating coefficients. If hardware fixes or modifications are applied during the season, separate calibration coefficients are required for each configuration used during a season.

There are a variety of types of targets in addition to ocean data that can be used for calculating equalization coefficients.

1) Land ice surface returns are plentiful but can give poor coefficients if the surface is saturated or affected by transients (e.g. the TR switches used for a number of seasons had slow switching times). A smaller affect is that the far field assumption becomes less accurate as the platform flies closer to the surface. For example, an error of almost 1° in the direction of arrival occurs when flying at the nominal altitude of 500 m.
2) Bedrock returns are rougher on a small scale but still provide quality coefficients if they are smooth with only small slopes over larger distances. Some good examples are shown in Figure 4-9 and Figure 4-10.

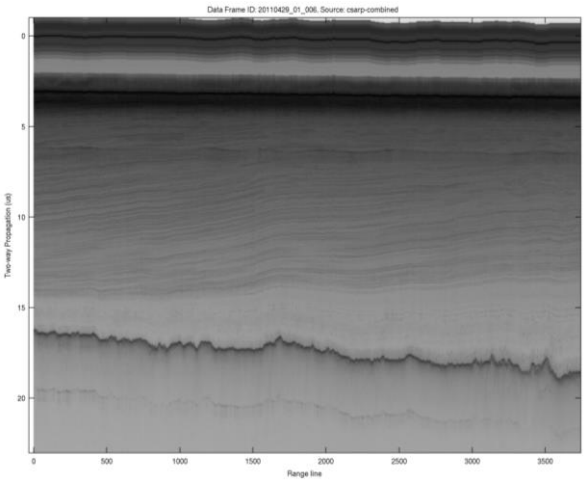

Figure 4-9: Example of good bedrock target from 20110429_01_006.

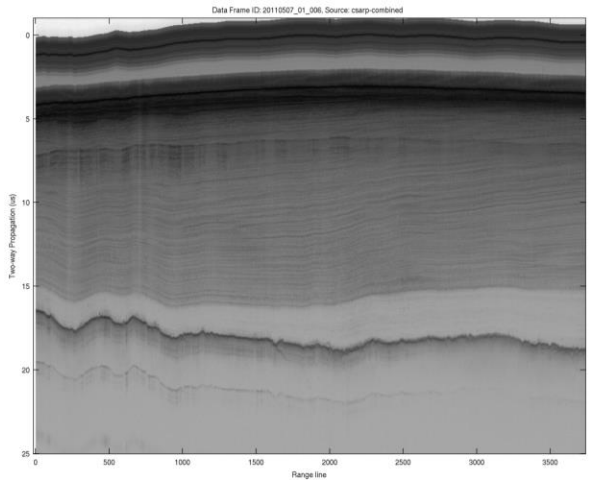

Figure 4-10: Example of good bedrock target from 20110507_01_006.

3) Internal layers can be used as well but must have good SNR and small dip angles in order to be isolated from other similarly strong adjacent internal layers. Examples are shown in Figure 4-11 and Figure 4-12. Internal layers can also be used to verify consistency between coefficients obtained from high-gain and low-gain waveforms.

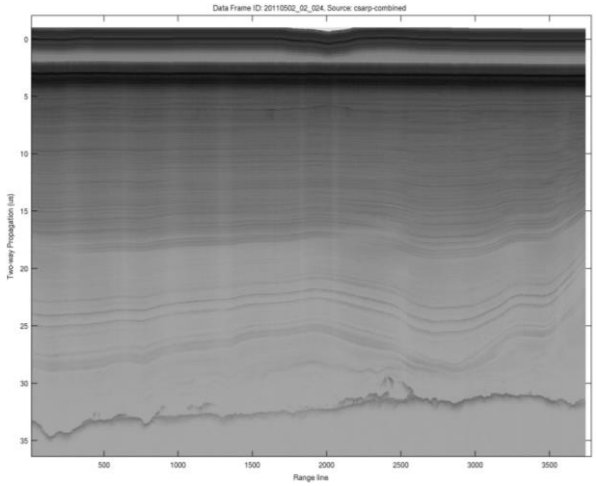

Figure 4-11: Echogram of data from 20110502_02_024 used to check calibration coefficients obtained from internal layers.

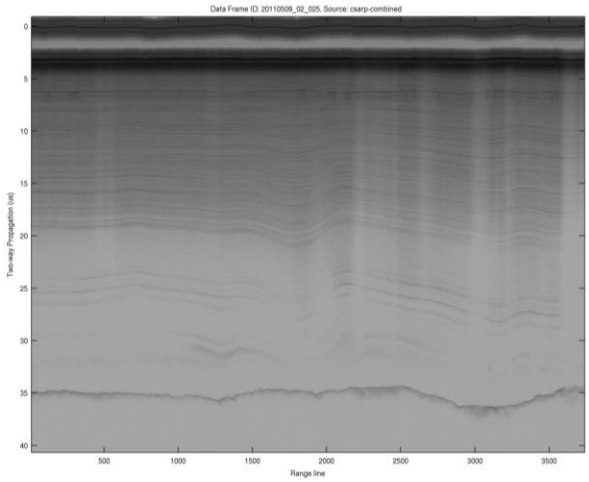

Figure 4-12: Echogram of data from 20110509_02_025 used to check calibration coefficients obtained from internal layers.

4) Whenever part of the radar transmit or receive chains are modified in the field a separate ocean calibration flight should be conducted. This will capture data to determine required channel equalization coefficients for all subsequent flights. Late in this season channel 14 was replaced due to malfunction. A calibration flight was flown on 20110512 to recalibrate the radar.

Table 4-7 and Table 4-8 show the amplitude and phase coefficients for the center 7 elements of the P3 array for a variety of data from different locations and including different targets than the reference data set. The highlighted row at the top of each table show the reference values. Below are the comparison coefficients and their relative offsets from the reference coefficients. The average offset and standard deviation of the coefficients are also shown.

Only column with RMS values of the errors and two new rows with mean and std of values across targets.

Table 4-7: Amplitude coefficients and relative offsets in dB.

ocean (ref)	3.3	1.6	0	-4.3	0.3	1.5	0	RMS error
ocean	2.7 (-0.6)	0.4 (-1.2)	0 (0)	-4.5 (-0.2)	0 (-0.3)	0.4 (-1.1)	-0.4 (-0.4)	0.69
ocean	3.5 (0.2)	1.7 (0.1)	0 (0)	-2.8 (1.5)	0.2 (-0.1)	1.2 (-0.3)	0.2 (0.2)	0.59
internal	2.3 (-1)	0.4 (-1.2)	0 (0)	-3.1 (1.2)	-0.8 (-1.1)	0.2 (-1.3)	-1.3 (-1.3)	1.10
internal	2.5 (-0.8)	0.3 (-1.3)	0 (0)	-3.8 (0.5)	-0.5 (-0.8)	0.2 (-1.3)	-0.8 (-0.8)	0.89
bedrock	2.7 (-0.6)	1.1 (-0.5)	0 (0)	-3.9 (0.4)	-0.2 (-0.5)	0.5 (-1)	-0.4 (-0.4)	0.56
bedrock	3.2 (-0.1)	1.7 (0.1)	0 (0)	-3.2 (1.1)	0.5 (0.2)	1.4 (-0.1)	0.3 (0.3)	0.44
surface	4.1 (0.8)	4.8 (3.2)	0 (0)	-2.7 (1.6)	0.1 (-0.2)	-0.1 (-1.6)	-1.7 (-1.7)	1.64
mean	3.0	1.49	0	-3.42	-0.1	0.54	-0.54	
std	0.64	1.58	0	0.66	0.44	0.55	0.73	

Table 4-8: Phase coefficients and relative offsets in degrees.

ocean (ref)	1.7	-36.6	0	9.8	6.4	-19.8	-8.2	RMS error
ocean	7.1 (5.4)	-32.6 (4)	0 (0)	20.5 (10.7)	9 (2.6)	-17.4 (2.4)	-6 (2.2)	5.03
ocean	-1.1 (-2.8)	-34.8 (1.8)	0 (0)	41.7 (31.9)	10 (3.6)	-14.2 (5.6)	-3.5 (4.7)	12.51
internal	0.4 (-1.3)	-36.9 (-0.3)	0 (0)	20.4 (10.6)	-1.6 (-8)	-22.9 (-3.1)	-9.8 (-1.6)	5.21
internal	3.2 (1.5)	-29.6 (7)	0 (0)	30.4 (20.6)	3.9 (-2.5)	-16.6 (3.2)	-4.4 (3.8)	8.51
bedrock	0 (-1.7)	-31.6 (5)	0 (0)	22.2 (12.4)	10.2 (3.8)	-10.7 (9.1)	-0.3 (7.9)	6.98
bedrock	-6.5 (-8.2)	-39.6 (-3)	0 (0)	19.9 (10.1)	11.7 (5.3)	-9 (10.8)	1.6 (9.8)	7.74
surface	-2.1 (-3.8)	-41.2 (-4.6)	0 (0)	19.6 (9.8)	3 (-3.4)	-19 (0.8)	-5.1 (3.1)	4.68
mean	0.11	-35.19	0	25.0	6.6	-15.69	-3.92	
std	4.23	4.27	0	8.29	4.90	4.81	3.75	

Table 4-9 shows the improvement in SNR for each type of target including a crossing of the Jakobshavn outlet glacier. The expected improvement in SNR based on the matched filter coefficients was 2.48 dB but we only see improvements of .1-.2 dB in actual data.

Table 4-9: SNR improvement in dB from equalization for various data sets.

	20110409_08	20110512_04	20110502_02	20110507_01	20110429_01	20110406_01
	(ocean – ref)	(ocean)	(internal layer)	(bed)	(bed)	(Jakobshavn)
Normal	88.83	84.45	49.71	65.48	69.60	42.57
Phase	89.21 (+.38)					
Match Filtered	88.93 (+.10)		49.91 (+.20)			
Phase & Amp	87.94 (-.89)					
Phase & MF	89.76 (+.93)					
Phase, Amp, MF	90.04 (+1.21)	87.18 (+2.72)	49.99 (+0.28)	65.82 (+.34)	71.88 (+2.27)	44.12 (+1.55)

4.10. **Sub-Array Processing**

4.10.1. 2011 Greenland P3 Antenna Array Configuration

The P3 carries 15 VHF bow-tie antennas in three sub-arrays. As shown in Figure 4-13, there are four elements on each wing which are receive only and seven on the fuselage which are both transmit and receive. The antennas in each sub-array are spaced $\sim\frac{\lambda}{2}$ $(.77\ m\ @\ 195\ MHz)$ apart. There is 4.75 m between the edge of the center and the wing arrays phase centers and 6.42 m between center and wing array phase centers and 12.85 m between the phase centers of the outer arrays. The actual array geometry is twice as large since the phase centers are the average of the transmit and receive positions. For example, the outer arrays are 2 times 12.85 or 25.7 m apart.

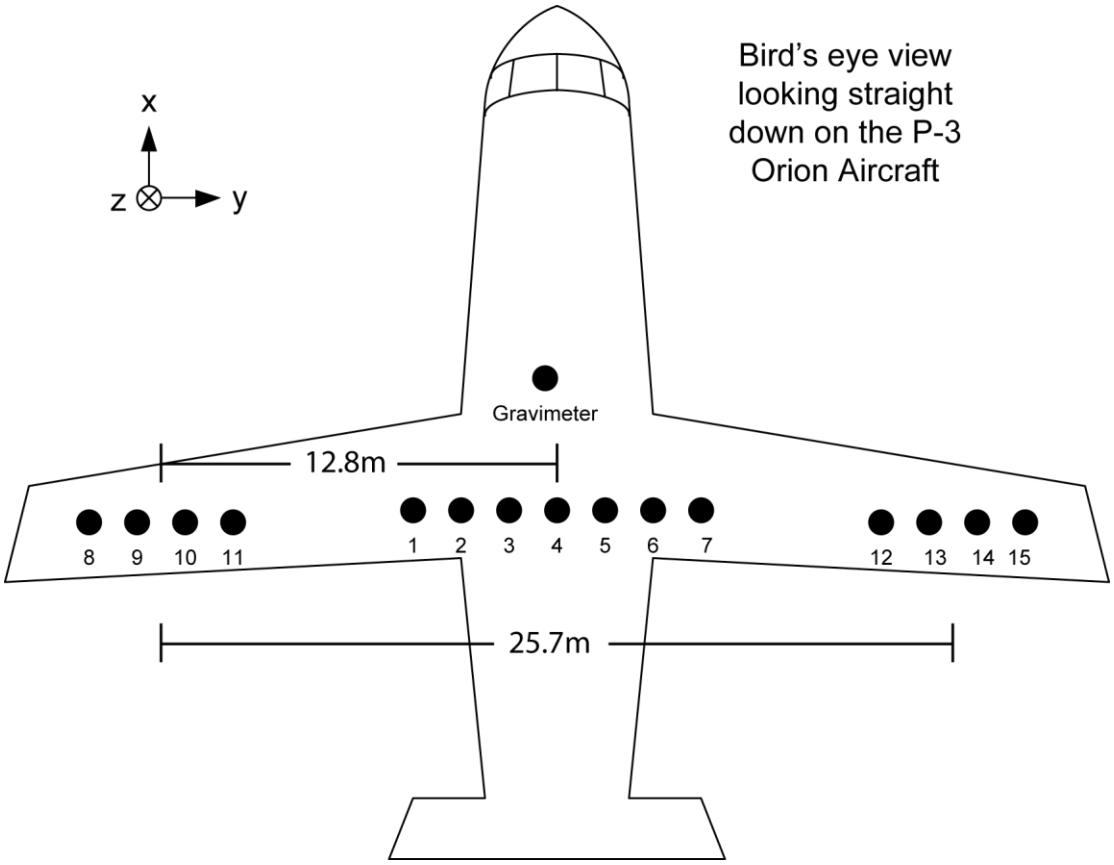

Figure 4-13: 2011 Greenland P3 antenna layout.

4.10.2. Limitations

There are several factors that limit the ability to coherently combine the data from all 15 antenna elements. First of all, the baseline between the phase centers of each sub-array is large considering we are looking primarily at nadir targets. This large baseline will result in baseline decorrelation, when phases from a target are more than 2π out of phase when received by two or more sub-arrays. For a radar altitude with $H = 500m$ and a target depth of $T = 2000m$ below the ice surface, the effective range to the target is $R = H + \frac{T}{\sqrt{\epsilon_{ice}}} = 1627m$. Then the pulse limited resolution of the nadir cell in the across-track dimension is $\sigma_{y,g} = 2\sqrt{\frac{Rc}{B}} = \sqrt{\frac{1627 \cdot 3x10^8}{30x10^6}} = 255m$. The critical angle, which would cause returns from the target to be more than $\frac{\lambda}{2}$ out of phase with each other, is $\theta_c = \sin^{-1}\left(\frac{\lambda}{2\sigma_{y,g}}\right) = \sin^{-1}\left(\frac{1.54}{2 \cdot 255}\right) = 0.17°$. This makes the critical baseline $B_{\perp_c} = \theta_c R = 0.17 \cdot 1627 = 4.91m$. So the results from antenna elements or sub-arrays that are farther apart than 4.91 m will be decorrelated. Thus the results from the center and wing sub-arrays (6.42 m displacement) and the left and right wing sub-arrays (12.85 m displacement) will most likely not combine coherently.

The second, related, factor that limits the usefulness of combining all 15 elements is the grating lobes in the array pattern when elements outside of one sub-array are combined. Figure 4-14 shows the array pattern created by three different groups of antenna elements. First the array for the center seven elements shows a wide main lobe with the first nulls beyond 15°. When the next adjacent elements of the outer sub-arrays are added, grating lobes appear around 7°. The 3 dB power point for this array pattern comes around 8°. From -8° to 8° the array power is reduced by 1.84 dB when elements 11 & 12 are added and 3.68 dB once all 15 elements are included. For a distributed target this means the array gain is lost by a decrease in the effective area of the target and because of the grating lobes the improved resolution is ambiguous.

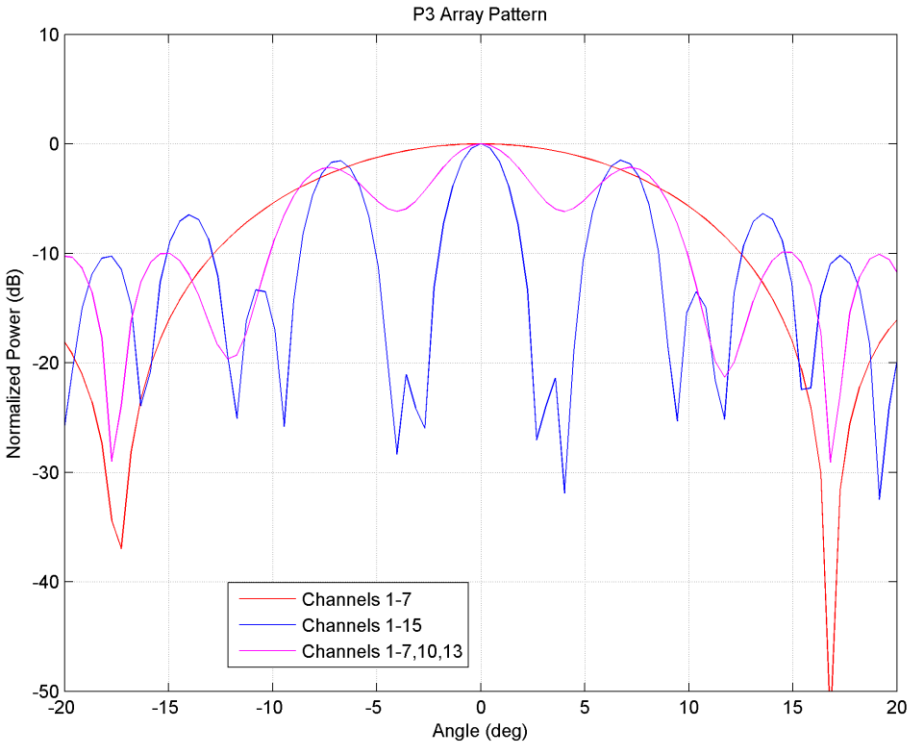

Figure 4-14: P3 array pattern using 1) center sub-array, 2) center sub-array plus next adjacent antennas, 3) all 3 sub-arrays.

Figure 4-15 shows the theoretical and actual SNR gain from combining between 1 and 15 of the P3 elements. The black line shows the ideal case where the signal from all elements are identical (the case of a single point target). The red line takes into account the noise powers as calculated by the noise covariance matrix and equal signal power. The cyan line shows the matched filter result accounting for the noise covariance (still for the single point target though). The blue circles show the actual SNR gain obtained with no channel equalization or matched filtering and the green x's include channel equalization and matched filtering. The first seven data points are the combination of the center seven elements, then the left sub-array, and finally the right sub-array.

It is clear that there is a decrease in SNR once the outer sub-arrays are included. Ideally, once the resolution refinement begins to limit the SNR due to a decreasing target size, the SNR would level off on average. The decrease in SNR is likely due to phase errors between the sub-arrays although the decrease is fairly small.

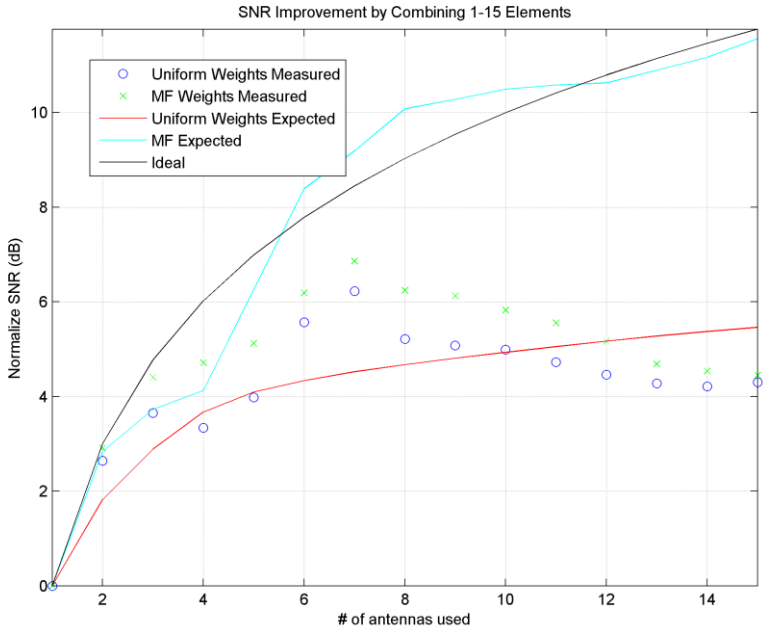

Figure 4-15: Coherent combination of 1 to 15 elements of the P3 array.

Even though all three sub-arrays probably do not provide much benefit when combined coherently with standard beam-forming, the arrays are still useful for incoherent averaging and performing tomography or interferometry on the collected data because of the large baseline between the sub-arrays. The particular imaging geometry where the large baseline is beneficial is for side looking imaging where layover is not an issue and there really is only one target in the range cell.

5. Optimal Processing Parameters

This section looks at some of the most important processing parameters and how they should be handled when processing data. These parameters include types of windows used to filter the data in fast-time and slow-time as well as along-track beamwidth used in the azimuth compression. These parameters have significant effects on our ability to detect or resolve targets and should be chosen carefully depending on the goals of data processing.

5.1. SAR Aperture/Along-track Resolution

The synthetic aperture for a target is the along-track distance over which that target's scattered signal will be used during processing. The maximum synthetic aperture is determined by the along-track beamwidth of the real antenna used in collection and the target scattering characteristics. A shorter synthetic aperture is often used for several reasons but the optimal synthetic aperture length to use is dependent on geometry, target characteristics, method of processing, and desired along-track resolution.

Unfocused SAR processing uses only portions of the SAR aperture where the phase of a target changes by less than 90°. Beyond 90° the signals begin to destructively interfere with each other until they completely cancel each other out at 180°. The unfocused SAR aperture is range and wavelength dependent as

$$L_{unfocused} = \sqrt{\frac{\lambda R_0}{2}}, \tag{47}$$

where

R_0 is the range of closest approach between the radar and the target.

A better option is to use some form of migration algorithm, like f-k migration (section 3.4.4), to extend the range over which the records can be coherently integrated constructively. This is called focused SAR and once the data have been migrated the only limits to the SAR aperture length are along-track antenna beamwidth, platform motion errors, and signal attenuation.

Platform motion errors deform the geometry of the acquired data causing phase errors in the migrated data. Ideally motion errors have already been removed at this stage in the processing via the methods described in section 3.4.3.

Similarly, once the data is attenuated to the point where the thermal noise floor has a significant effect on the received signal the addition of this data will add more phase errors to the results.

Based on a simulation for the P3 center array (appendix F, Emily Arnold, personal communication, March 29th, 2013), the full along-track beamwidth is 120° (±60° centered around nadir) as measured by the 3 dB point of the array pattern of the center sub-array. For

reference, using a platform height of $h = 500\ m$ and a target depth of $R_0 = 1500\ m$ gives an along-track footprint of 3,409 m.

Table 5-1: Potential SNR improvement of focused vs unfocused azimuth compression.

	Unfocused	Focused
h	500 m	500 m
R_0	1500 m	1500 m
L	34 m	130 m
Δ_x	0.324 m	0.324 m
N_x	105	401
Integration Gain	20.2 dB	26.0 dB

An example of the potential for improvement of focused over unfocused SAR (parameters in Table 5-1); at $R_0 = 1500\ m$ and $\lambda = 1.53\ m$ the unfocused SAR aperture is $L_{unfocused} = 34\ m$. A typical average P3 velocity is 135 m/s with 24 presums. This gives an along-track record spacing of

$$\Delta_x = \frac{v \cdot presums}{f_{PRF}} = \frac{135 * 24}{10000} = 0.324\ m.$$

This means there are a maximum of $L_{\text{unfocused}}/\Delta_x = \frac{34}{0.324} \approx 105$ records that can be coherently integrated to improve the SNR. The SNR gain from coherent integration is a factor of the number of records integrated N_x so the maximum SNR gain is 105 or 20.2 dB. Alternately using focused SAR with a desired along-track resolution of 5 m, the SAR aperture is 130 m or 401 records (from equation (35)). This raises the maximum SNR gain to a factor of 401 or 26.0 dB, an increase of 5.8 dB over unfocused SAR. The along-track resolution is proportional to the ratio of target range to aperture length. When we are sounding a distributed target the increase aperture length will not lead to improved SNR, the reasons for which will be discussed in the next section and appendix G. Both the focused and unfocused SAR aperture lengths that are used during our processing are much shorter than the along-track aperture length of the antenna array so there is no need to take the along-track antenna beamwidth into consideration further.

5.1.1. Simulation

To test the relationship between SAR aperture length and SNR, simulated data of a single point target was processed using a series of synthetic aperture lengths which doubled from one to the next. Since the number of records stays constant between processed data sets the effect of doubling the aperture is to double the number of records, N_x, used which should increase the SNR by a factor of 2 (3 dB). Figure 5-1 shows the simulation results which are very close to the theoretical results.

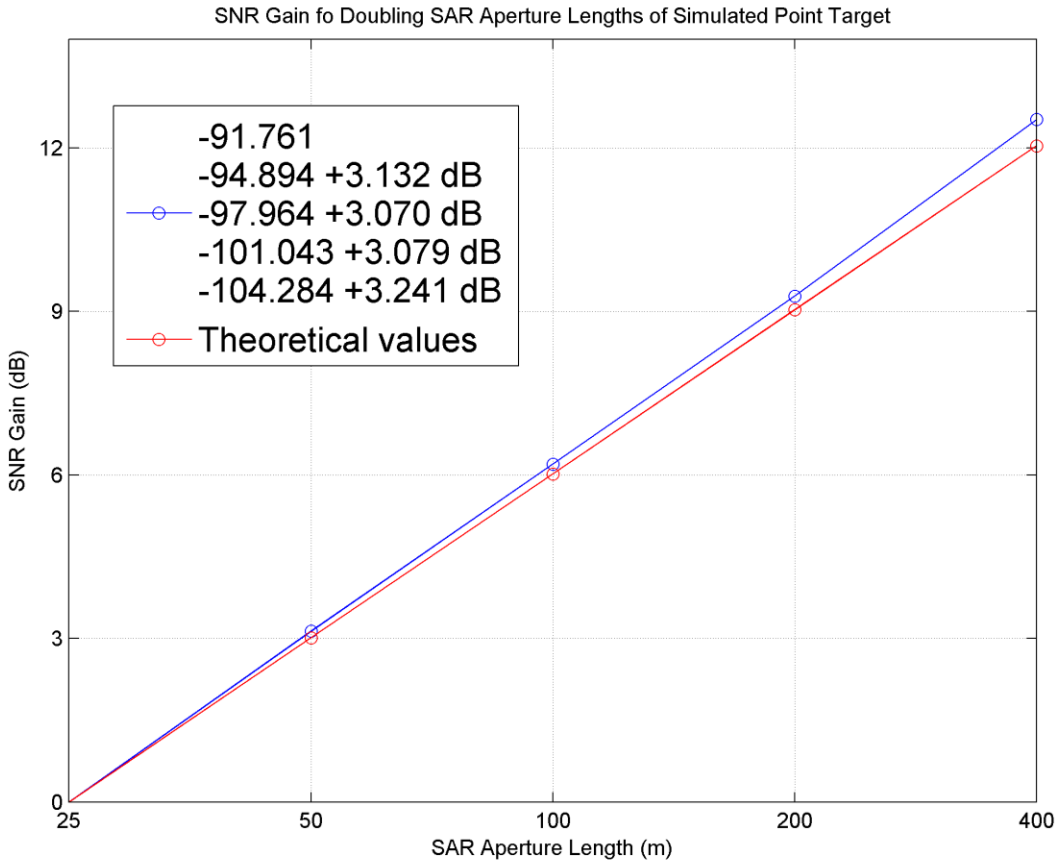

Figure 5-1: SAR aperture length vs SNR simulation results.

5.1.2. Depth Sounder Data

When using depth sounder data the response generally comes from a distributed target rather than a point target. The way a distributed target's response changes with respect to SAR aperture is different than that of a point target. This is because doubling the aperture splits the resolution cell in half. Theoretically a point target is infinitely small so splitting the resolution cell size in half results in one resolution cell with full signal power and one with only noise power. If they were split again there would still be one cell with full signal power and three with noise power.

If we assume the signal power is evenly distributed across the Doppler spectrum, then splitting the resolution cell of a perfectly distributed target in half results in two smaller cells with the same SNR as the original. However, the signal power is not evenly distributed along the Doppler spectrum (exampled in Figure 5-3 and Figure 5-5). As the angle off nadir increases, additional path loss and target backscatter roll-off will reduce the SNR gain so that each split resolution cell will have less than the original resolution cell. At some angle the backscatter will drop to zero and there will be serious SNR degradation as only noise is added to the SAR response. Finding the optimal angles over which to integrate the SAR response requires

knowing where the energy is coming from and understanding the required along-track resolution. Because the radar is moving and has a wide along-track beamwidth we can use its Doppler spectrum to determine which along-track direction the energy is coming from.

Plotting data in the range-Doppler domain can help determine where energy is coming from for a frame of data. The Doppler spectrum is related to the signal's angle of arrival via the along-track wavenumber. The range-Doppler domain is created by applying an FFT to the data in the x-dimension, converting from along-track distance to along-track wavenumber. The along-track wavenumber can be converted to angle of arrival via equation (48).

$$\theta_i = sin^{-1}\left(\frac{k_x}{k}\right), \tag{48}$$

where

k is the wavenumber of the transmitted signal,

k_x is the along-track wavenumber of the transmitted signal.

Each pixel of the range-Doppler echogram (as shown in Figure 5-3 and Figure 5-5) represents the reflected power at a particular range and incident angle. The column at the center of the echogram represents power reflected from nadir (0° incident angle) and the left-most and right-most columns represent the reflections from the maximum negative and positive angles, respectively. The energy distribution can be tracked by determining the SNR of the target in each Doppler bin. The SNR is defined as the ratio of the average power in a window around the target return for a single Doppler bin to the average power of a large swath of noise data covering the entire data set. As the Doppler frequency (angle of arrival) increases we expect a decrease in SNR for a nadir looking radar due to travel path attenuation and decreasing target backscatter (for smooth surfaces).

Fitting a line from the peak SNR value to 10 degrees on either side of the peak gives an average roll-off per degree for the data set. Examining the data distributions for different radar-target geometries we find that reflected power roll-off is usually in the range of .1-.3 dB per degree over the ten degrees on either side of the peak SNR value.

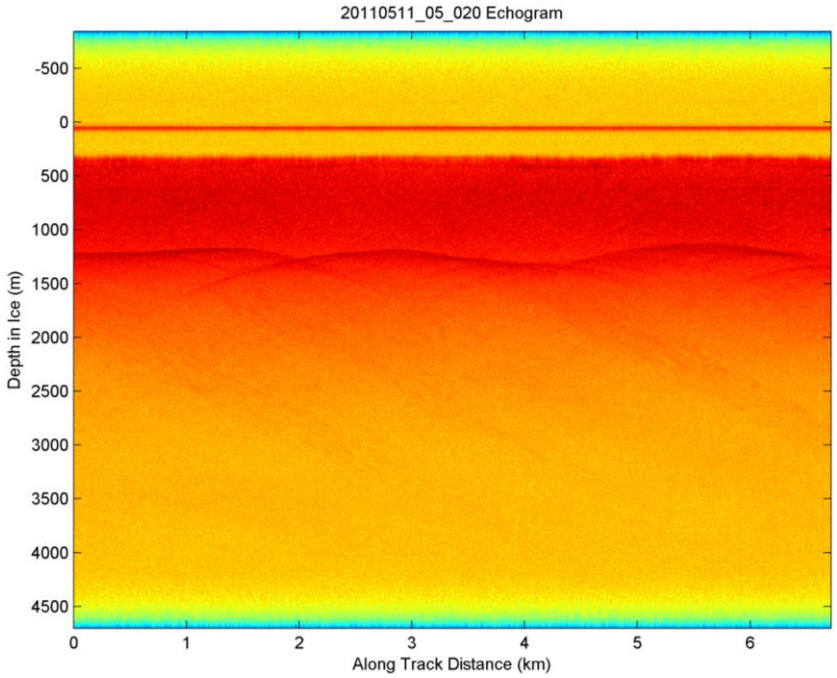

Figure 5-2: Example of medium depth ice over rolling bedrock.

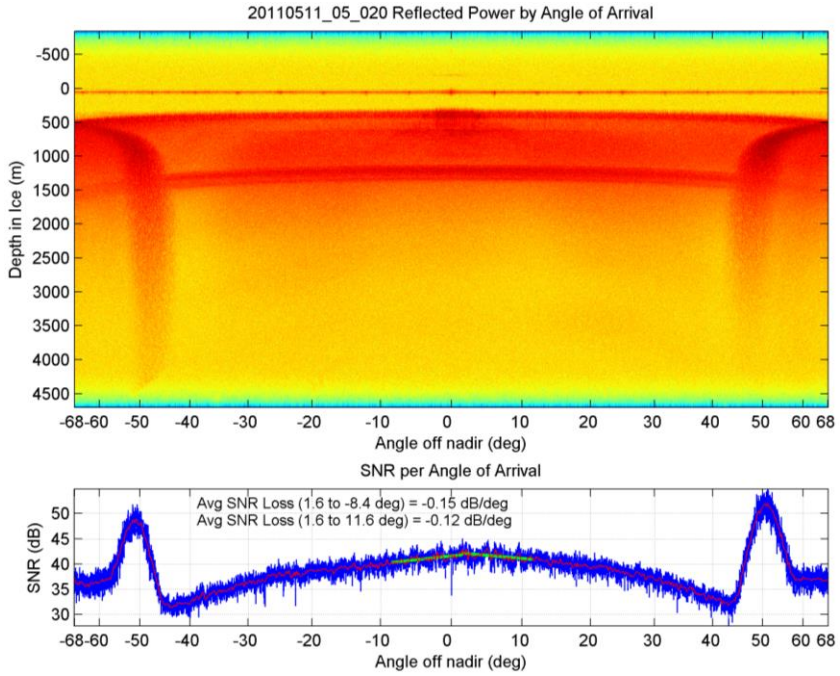

Figure 5-3: Above: Doppler spectrum of echogram in Figure 5-2. Below: Distribution of energy from a medium depth, undulating reflector as a function of incident angle. The increase in power on the edges at ±50 deg is due to aliased surface clutter energy.

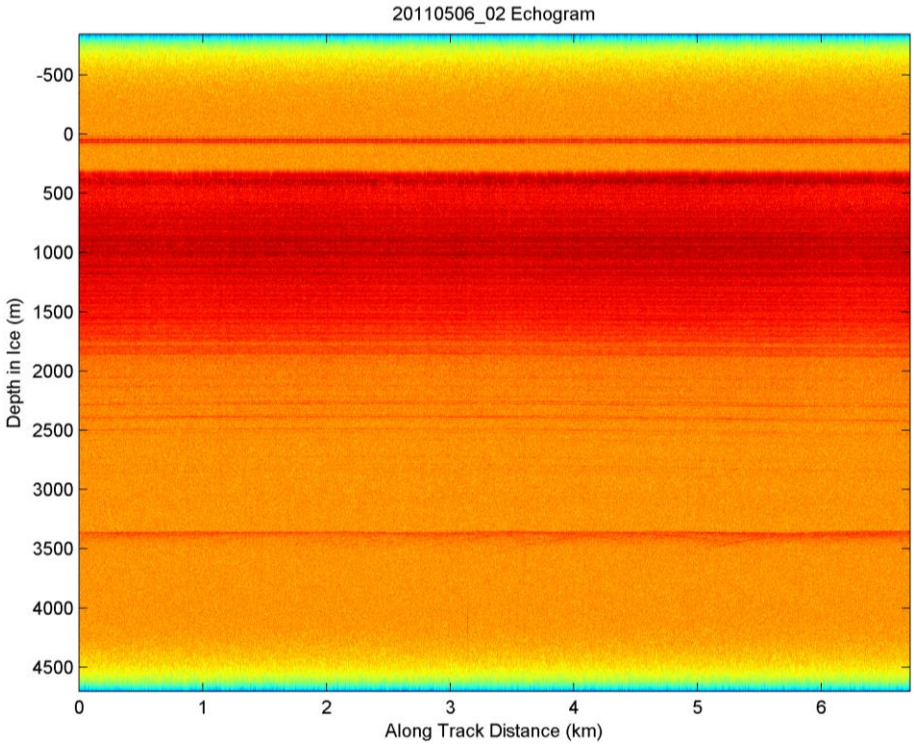

Figure 5-4: This is an example of deep, flat bedrock.

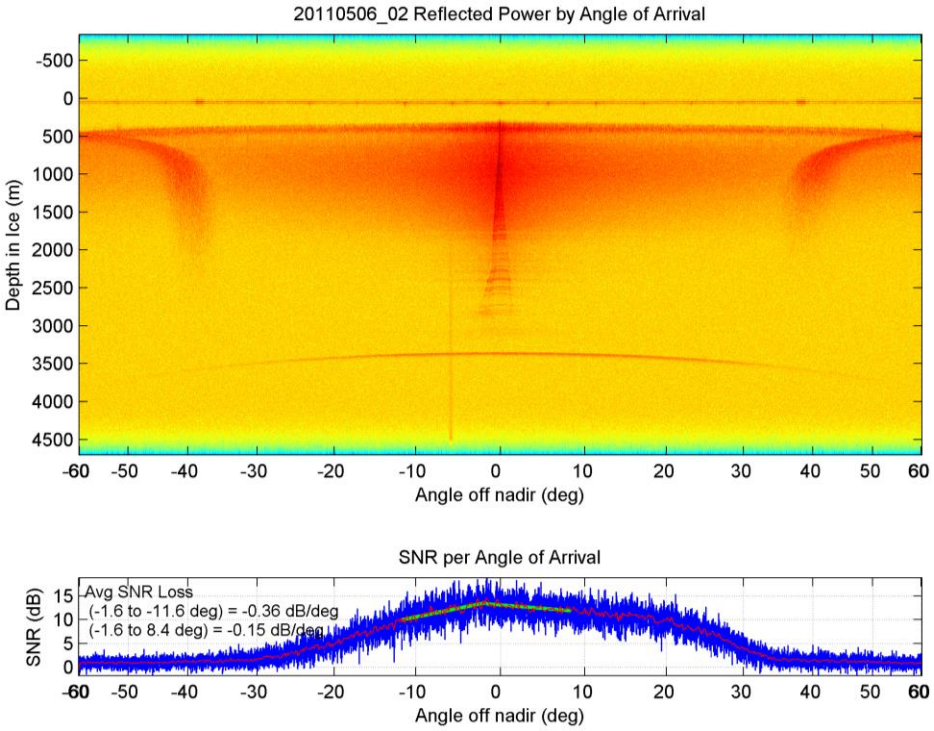

Figure 5-5: Above: The profile from Figure 5-4: This is an example of deep, flat bedrock. in the range-Doppler domain. Below: Distribution of energy from a deep, flat reflector as a function of incident angle.

As long as the peak SNR is reasonably high even a .3 dB per degree loss in SNR should not restrict the Doppler bins that can be used in migration. However, unless amplitude compensation is applied, the resolution will not improve substantially once the Doppler roll-off is more than a few dB. When processed the data show a similar story. Table 5-2 shows the average SNR in the depth/along-track domain for the data segment in Figure 5-4. We see a gradual drop in SNR with a drop of 6.64 dB up to a full beamwidth of 40 degrees (or an along-track resolution of 1.1m). This is not a particularly difficult segment of bedrock to detect but a good baseline.

Table 5-2: SNR Change vs SAR Aperture Length (20110506_02_002)

SAR Aperture (m)	13.6	27.3	68.3	136.7	274.6	415.4	560.4
Full Beamwidth (deg)	1	2	5	10	20	30	40
Ideal Along-track Resolution (m)	44.0	22.0	8.8	4.4	2.2	1.5	1.1
SNR (dB)	74.56	74.30	73.26	72.14	70.37	69.04	67.92
SNR Change (dB)	0	-0.26	-1.04	-1.12	-1.77	-1.33	-1.12
“Added Noise” SNR Change (dB)	0	-3.03	-3.98	-3.01	-3.03	-1.80	-1.30
% Noise	NA	11.6%	35.5%	45.5%	66.6%	77.7%	87.9%
Total SNR change (dB)	0	-0.26	-1.30	-2.41	-4.19	-5.52	-6.64
SNR change per degree (dB)	0	-0.26	-0.35	-0.22	-0.18	-0.13	-0.11

Looking at the data another way: what happens if we assume that each time we increase the SAR aperture length that the added Doppler bins contain only noise with no signal component? This is calculated in row 6 of Table 5-2. The percentage of noise in the added Doppler bins indicates how much signal there is in the added beamwidth. A larger percentage indicates that added

Doppler bins contain low SNR data. When the percentage rises to 100% there is no signal present in the added Doppler bins. The results in row 7 show that as we increase the SAR aperture the percentage of noise rises significantly after widening the beamwidth to two degrees and that the signal power is largely concentrated within five degrees, where the noise percentage is around 1/3 or less. Unless a finer resolution is required it is not recommended to increase the beamwidth. It would be more productive to increase the aperture through subaperture multilooking (which should be weighted according to the SNR of each look).

5.2. **Windowing**

5.2.1. Sidelobes and Window Functions

In signal processing, sidelobes, or spectral leakage, come from the combination of the received signal and a window function. This is the case with any matched filtering process, which is the basis of each step of processing CReSIS depth sounder data. The matched filters used in range compression, azimuth compression, and array combination are designed to improve the SNR and resolution but they cause energy from the main lobe of the signal's spectral response to "leak" into adjacent spectral components.

This leakage is worst when there is an abrupt transition at the edges of the filter. Since any band-limited signal is an infinite signal combined with a rectangular window, this is the worst-case scenario for spectral leakage sidelobes. The sidelobes can be suppressed by tapering the edges of the window in the frequency domain, although this leads to a widening of the main lobe in the time-domain.

Due to this trade-off between sidelobe level and main lobe width it is important to understand the data content and desired product of the processing. For example, if there are multiple targets of interest very close together, several internal layers for example, then using a window function that produces a very wide main lobe could make it difficult to resolve the targets. If, on the other hand, the desired target was a layer near the bedrock, using a sidelobe suppressing window should be used so the target layer is not masked by the bedrock sidelobes.

Windows can be applied to a signal in any domain: time, frequency, space, or wavenumber. A window applied in one domain helps suppress sidelobes that can raise the noise floor and mask smaller targets in the opposite domain. Windows help decrease the correlation between widely separated spectral components in the opposite domain (i.e. lowered sidelobes) at the expense of increasing correlation between closely separated components which leads to mainlobe widening.

5.2.2. Window Properties

Due to the importance of preserving phase information in the processing, FIR filters are used to window the data. To minimize sidelobe levels, while minimizing energy loss due to tapering, a Tukey window is used. The Tukey window is a tapered cosine window that is a convolution between a cosine window and rectangular window. A taper parameter R determines the ratio of the rectangular window to the cosine window. When R=0 the Tukey is equivalent to a

rectangular window while R=1 is equivalent to a Hanning window. R=.5 would be an even ratio of constant rectangular window to cosine taper. The choice of taper parameter for a chirped pulse is determined by the desired peak sidelobe level (PSL) and the integrated sidelobe level (ISL). The PSL is the ratio of the magnitude of the strongest sidelobe to the magnitude of the main lobe, and the ISL is the ratio of the integrated power of the sidelobes to the power of the main lobe. Analysis by Li [1] shows that the best performance of both PSL and ISL for a 10us pulse with 30 MHz bandwidth occurs when the taper parameter is set to R=0.1.

5.2.3. Window Application

Window functions can improve data in both the range and along-track dimensions. In the range dimension they suppress sidelobes caused by pulse compression. The 2011 Greenland P3 mission alternately transmitted 1 and 10 us pulsed chirps with a 0.2 Tukey taper applied in the time-domain. The taper value was determined by simulation [1]. This analysis only uses the 10 us data since it most often contains the bedrock reflection. To minimize sidelobes the received signal requires the matched filter for pulse compression to have a matching 0.2 Tukey taper, also in the time-domain. A window can be applied to the frequency-domain received signal in the range dimension to further suppress sidelobes close to the main lobe in the time-domain.

A window applied in the wavenumber-domain will suppress close in sidelobes in the along-track dimension. The window is applied after selecting Doppler bins to be used for migration. Returns from larger angles may still have useful information but also include more noise. This window will suppress large angle returns without removing them altogether. This window will also affect along-track sidelobe levels when transforming the data back to the time-domain at the end of the f-k migration process.

5.2.4. Effect on Real Data

To test the effect of windowing on a bedrock target, four windowing scenarios were used. A 10% Tukey window and a 100% Tukey window were applied in the fast time and slow time dimensions in each possible combination. The windows were applied in the frequency and wavenumber domains respectively. For the 100% Tukey window, the outer frequencies are weighted lower than the center frequencies. If the signal spectrum is flat, then SNR will be lost as the taper ratio increases. Ideally this is balanced out by suppression of sidelobes. If the signal spectrum is already tapered (e.g. as we saw in the case of the Doppler spectrum), the SNR may improve because the contribution of lower SNR portions of the signal is suppressed.

In the fast-time dimension the averaged A-scopes for each of the four cases are adjusted by their noise floor and plotted together. We see what seems like a slight widening of the target return for the 100% Tukey window in the fast-time dimension, as shown in Figure 5-7. The 100% Tukey consistently contributed an increase in SNR on the order of tenths of a dB. The expected -6 dB main lobe width increase, based on an ideal pulse simulation, would be 1.46 normalized bins, as shown in Figure 5-6. This should result in an almost 50% widening of the target main lobe for a point target. The widening in Figure 5-7 is masked due to the target backscatter roll-off

so the widening, in the case of the bedrock, may not be a significant concern. For internal layer tracking, widening could become more of a problem if two layers are close together and need to be resolved.

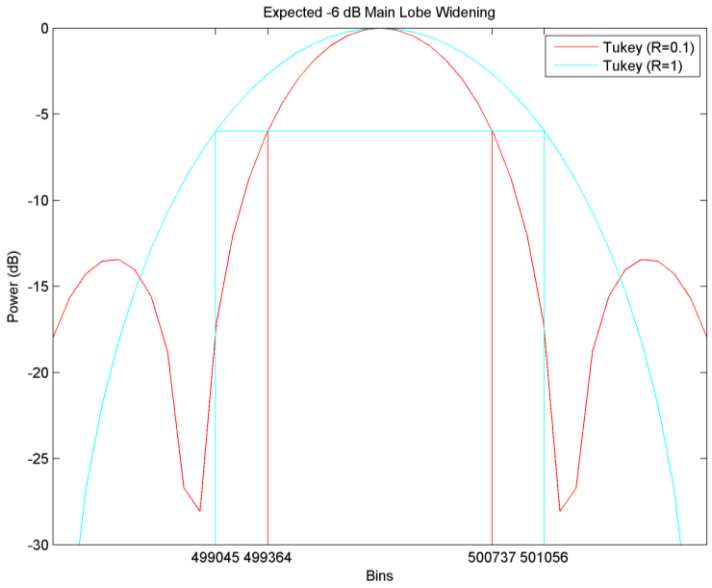

Figure 5-6: -6 dB main lobe widening simulation. The expected widening is by almost 50%.

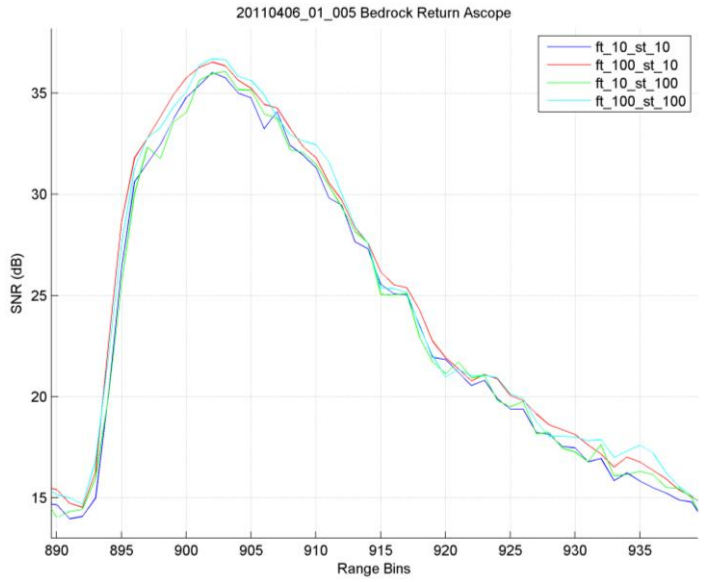

Figure 5-7: A sample of the bedrock return power for each windowing case, adjusted for the noise floor. It was averaged a across a section of data with high SNR to reduce variance.

To identify any change in SNR due to the effects of windowing a comparison of the SNR of the target return for each record is made. This will show any trends and the average of these SNR values for each data set show any overall improvement in SNR for the data set. As shown in the blue tiles in Table 5-3, 10% Tukey in both dimensions yields the lowest SNR, 100% Tukey in both directions yields the best results, and a combination of the two are in between. Since advanced processing is most important for bringing out weak signals, an average of SNR values over the weakest records can be more informative. Narrowing the SNR range down to 10-30 dB to look at the portion of the data with the weakest reliably detectable signals we see similar improvement. Figure 5-8 shows the SNR for each record in the data set.

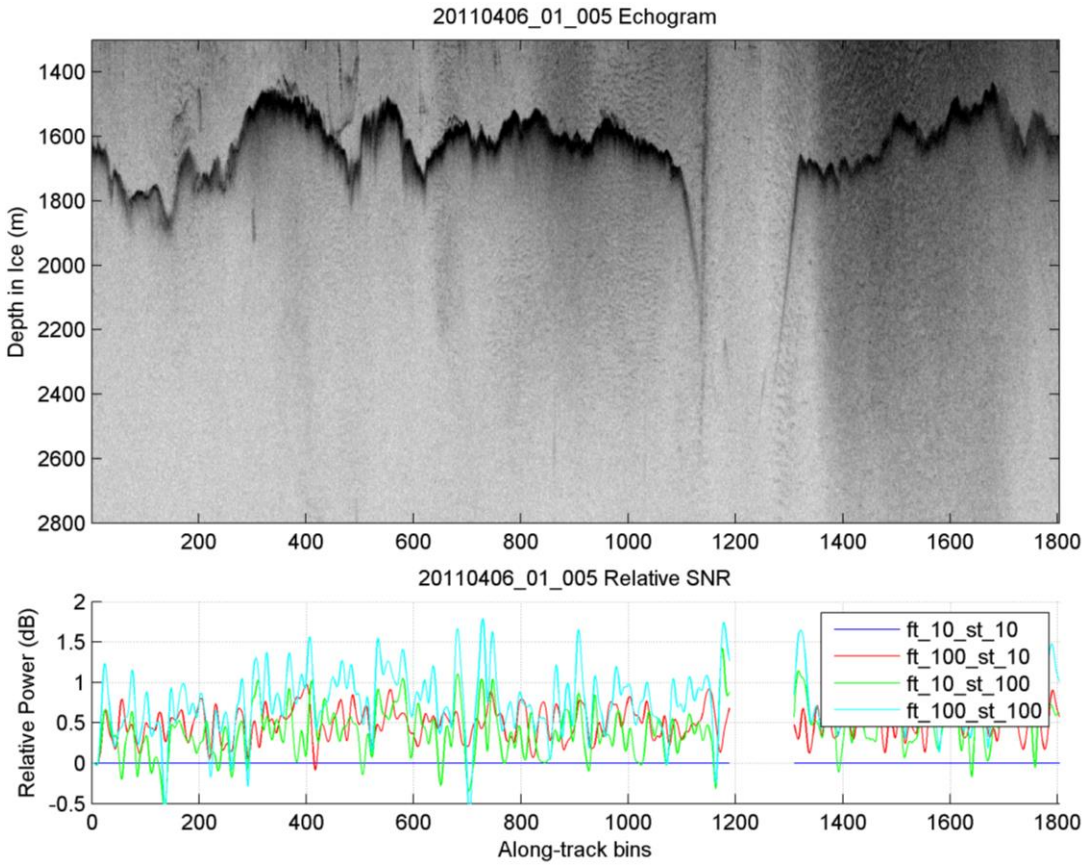

Figure 5-8: Above) An echogram with high and low SNR areas. Below) The SNR of the bedrock response for each record of the data (SNR relative to ft_10_st_10 case).

Table 5-3: SNR improvement, in dB, for different configurations of fast-time and slow-time windowing. Blue tiles include the whole SNR range, red tiles are limited only SNR's the fall within the 10-30 dB range.

	FT 10%		FT 100%	
ST 10%	0	0	0.51	0.50
ST 100%	0.43	0.65	0.83	0.99

5.3. **Relative Permittivity**

Using the correct relative permittivity of ice is important for precise focusing of the SAR data in the along-track dimension, as well as determining the actual target depth. In reality the relative permittivity of ice changes with its density and water content, however it is difficult to determine the relative permittivity without ice core analysis. The relative permittivity for pure ice that is used to make CReSIS data products ($\epsilon_r = 3.15$) was used for all other processing tests in this thesis with the assumption that this would provide the best processing results. To test whether this assumption is accurate a range of relative permittivity values was used for processing the same section of data multiple times.

The relative permittivity affects the along-track focusing via the refractive index $\eta_{ice} = \sqrt{\epsilon_{ice}}$ in equation (35). If the relative permittivity used is too small it will under migrate a point target hyperbola, creating a tighter but still uncollapsed hyperbola, and if too large it will over migrate it, creating an inverted hyperbola. Either case leaves the energy smeared over the surrounding pixels. This would be a larger issue when trying to detect only point targets, however, since we are dealing with a distributed target that will not collapse like a point target, the smearing of energy will mostly overlap with adjacent target smearing and result in little change in SNR. The relative permittivity also affects the conversion from target time delay to depth $d = \frac{t_d c}{2\sqrt{\epsilon_{ice}}}$, which is used to determine the ice thickness.

For each data set the bedrock is detected for each along-track bin then the SNR change is averaged over all the bins. The final average for each data set is compared to the baseline data set processed with $\epsilon_{ice} = 3.2$. The data used for testing is shown in the top of Figure 5-9. It was chosen since it has a large range of target depth values and target SNR. The bottom of Figure 5-9 shows that on a bin-by-bin basis the SNR relative to the baseline data set changes by less than ±0.5 dB over the profile. The average SNR change, shown in Figure 5-10, shows that in fact a constant relativity of $\epsilon_{ice} = 5.4$ provides the best overall results. The peak average SNR gain is less than 0.25 dB per bin which is negligible compared to other processing parameters.

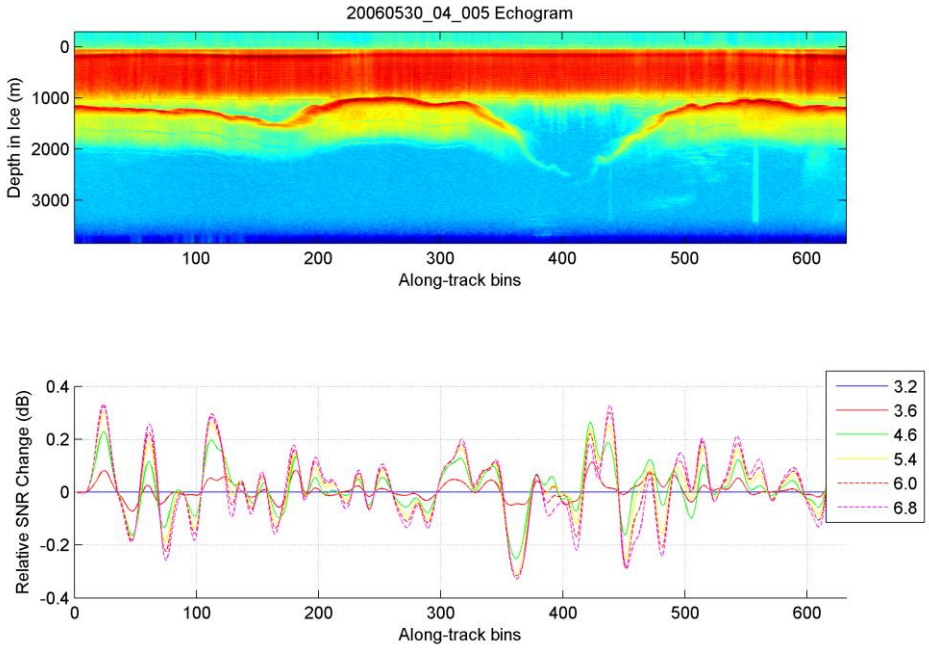

Figure 5-9: Top: Echogram of data used for analysis. Bottom: Relative SNR change of bedrock return.

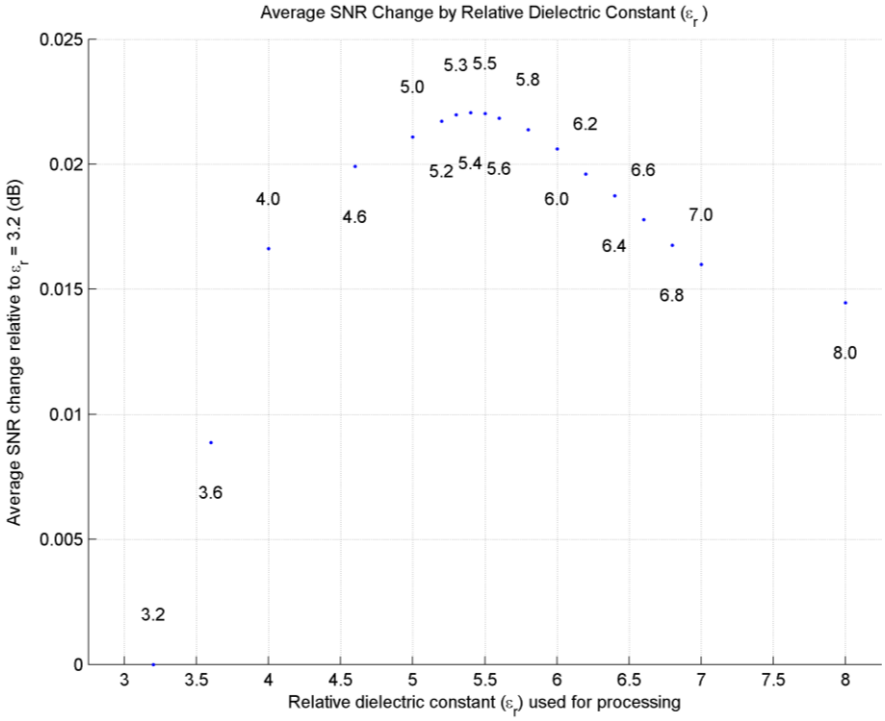

Figure 5-10: Relative total SNR change for various relative permittivity values.

6. Conclusions and Future Work

6.1. Conclusions

6.1.1. CSARP Validation

The range, azimuth, and array processing and lever arm application were all tested using simulated point target data with the results displayed in Table 6-1. The range and azimuth processing resulted in SNR gains within .15 dB of theoretical expectations. In the cross-track the ideal array combination resulted in exactly the expected SNR gain. The matched filtering applied to an array with different noise floors showed an improvement of over 1 dB when combined using a matched filter instead of a uniform filter. The lever arm application resulted in a slightly better than expected SNR gain, probably due to noise floor variations.

Table 6-1: CSARP verification results.

	Expected SNR Gain (dB)	Actual SNR Gain (dB)
Range Compression	18.75	18.90
Azimuth Compression	27.96	27.77
Array: Equal Noise – Equal Coeffs	6.02	6.02
Array: Diff Noise – Equal Coeffs	2.46	2.60
Array: Diff Noise – Matched Coeffs	3.58	3.68
Lever Arm Application	6.02	6.11

6.1.2. Channel Equalization & Matched Filtering

It was shown (in Table 4-7 & Table 4-8) that stable channel equalization coefficients for the seven receivers of the center array of the 2011 Greenland P3 mission could be obtained over a variety of targets including ocean surface, ice surface, internal ice layers, and bedrock. It was also shown that a combination of phase and amplitude corrections followed by matched filtering provides better results than any other combination of those three processes (Table 4-9).

6.1.3. SAR Aperture Analysis

While longer is better in terms of SAR aperture length for a point target (Figure 5-1), when it is a distributed target the SNR will drop as the SAR aperture length increases (Table 5-2), because the SNR falls off for larger Doppler frequencies. Even if the added Doppler bins have a high SNR, the SNR will, at best, stay constant due to the nature of subdividing the resolutions cells. Figure 5-3 & Figure 5-5 show the Doppler spectrums of flat and undulating bedrock and might be useful in informing sub-aperture processing parameters.

6.1.4. Dielectric constant analysis

Figure 5-10 shows that a dielectric constant of $\epsilon_r = 5.4$ produces better SNR on average over a data set than a dielectric constant of $\epsilon_r = 3.15$. The average improvement is only 0.025 dB so it

may not be significant. Further investigation into resolution improvements and isolated point targets should be conducted.

6.2. Future Work

6.2.1. CSARP Simulator

The CSARP simulator should be made adaptable for future versions of the radar. We recommend achieving this by modularizing it to allow outputs for any CReSIS acquisition format. Also the method for entering parameters should be refined and the functionality to handle multiple waveforms added.

We recommend that the simulator be modified to test clutter since clutter from channel walls is a major issue when sounding fast-flowing outlet glaciers. Adding a clutter simulator would provide the ability to isolate different aspects of clutter rejection algorithms to determine their effect on the data.

More advanced motion compensation abilities in the radar simulator would allow for the CSARP motion compensation algorithms to be validated. We recommend adding full attitude control in creating simulated data in order to validate the full motion compensation algorithms in CSARP.

6.2.2. Doppler Domain Analysis

Analysis of the Doppler spectrum of a data frame would be useful for appropriately weighting the sub-aperture combination when doing multi-look processing. We recommend further exploration of data analysis in the range-Doppler domain to determine the spectrum and skew or offset from nadir and the integration of these tools into the CReSIS toolbox.

We also recommend further testing of the application of an along-track window in regard to the desired final along-track resolution. Since windowing changes the main lobe width we currently obtain coarser along-track resolution than desired. Compensation for this widening should be included in CSARP processing.

References

[1] Li, Jilu, Mapping of Ice Sheet Deep Layers and Fast Outlet Glaciers with Multi-Channel-High-Sensitivity Radar, Dissertation, Department of Computer Science and Electrical Engineering, University of Kansas, 2010.

[2] Ender, J. and J. Klare. 2009. System architecture and algorithms for radar imaging by MIMO-SAR. *Radar Conference, 2009, IEEE*. 1-6. (10.1109/RADAR.2009/4976997).

[3] Ulaby F., Moore R., Fung A., "Microwave Remote Sensing. Active and Passive", Vol 2: Radar Remote Sensing and Surface Scattering and Emission Theory, p.461, Addison-Wesley Publishing Company, 1981.

[4] Legarsky J. J., Synthetic-Aperture Radar (SAR) Processing of Glacier-icedepth-Sounding Data, Ka-Band Backscattering Measurements and Applications, Dissertation, Department of Computer Science and Electrical Engineering, University of Kansas, 1999.

[5] F. Rodriguez-Morales, P. Gogineni, C. Leuschen, J. Paden, J. Li, C. Lewis, B. Panzer, D. Gomez-Garcia, A. Patel, K. Byers, R. Crowe, K. Player, R. Hale, E. Arnold, L. Smith, C. Gifford, D. Braaten, and C. Panton, "An Advanced Multi-Frequency Radar Instrumentation Suite for Polar Research," *IEEE Transactions on Geoscience and Remote Sensing*, June 2013.

[6] Ulaby F., Moore R., Fung A., "Microwave Remote Sensing. Active and Passive", Vol 3: From Theory to Application, p.2020, Addison-Wesley Publishing Company, 1981.

[7] Brandwood, B.A., A complex gradient operator and its application in adaptive array theory. IEE Proc., Vol. 130, Pts. F and H, No. 1, FEBRUARY 1983.

Appendix A: CSARP Simulator Instructions

The simulator is comprised of the static main simulator code,

csarp_simulator.m

the user editable setup code,

run_csarp_simulator.m

the user editable Excel spreadsheet,

csarp_simulator_param.xls (must be in "Microsoft Excel 5.0/95 Workbook" format)

and these dependent functions located in the cresis-toolbox,

physical_contstants.m

utc_leap_seconds.m

trajectory_with_leverarm.m

geodetic2ecef.m

ecef2lv.m

motion_comp.m

refraction.m

To run the CSARP simulator:

1) Make sure run_csarp_simulator.m is pointing to the correct csarp_simulator_param.xls spreadsheet
2) Edit the values in csarp_simulator_param.xls
3) Run run_csarp_simulator.xls

Appendix B: Two-Media Refraction Model Derivations

Ray Path

We know the position of the radar and the target but we don't know the path it will take to get there. This path, and subsequently the travel time, can be calculated using Snell's law. We must also know the height of the radar above the media interface and the depth of the target below the interface and the index of refraction for each medium.

Two-Media Refraction Model

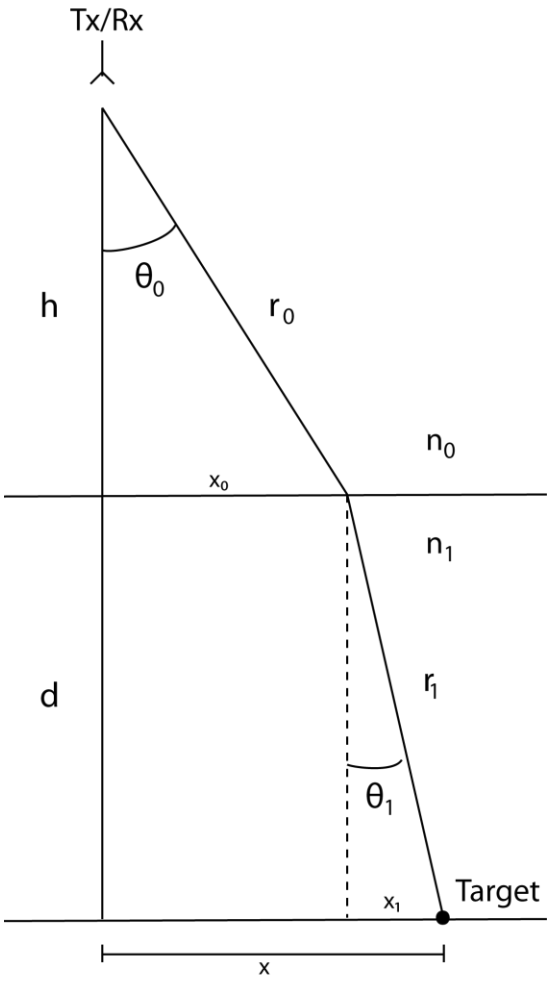

h: vertical distance above media interface
d: vertical distance below media interface
r0: ray path from source to media interface
r1: ray path from media interface to target
n_0 : index of refraction for media 1
n_1 : index of refraction for media 2
θ_0 : angle of arrival at media interface
θ_1 : angle of refraction at media interface

Snells's Law

$$n_0 \sin\theta_0 = n_1 \sin\theta_1$$

$$\sin\theta = \frac{x}{\sqrt{x^2 + y^2}}$$

$$n_0 \frac{x_0}{\sqrt{x_0^2 + h^2}} = n_1 \frac{x_1}{\sqrt{x_1^2 + d^2}}$$

Square both sides to remove square root

$$n_0^2 \frac{x_0^2}{x_0^2 + h^2} = n_1^2 \frac{x_1^2}{x_1^2 + d^2}$$

Remember $x_1 = x - x_0$

$$n_0^2 \frac{x_0^2}{x_0^2 + h^2} = n_1^2 \frac{(x - x_0)^2}{(x - x_0)^2 + d^2}$$

$$n_0^2 x_0^2 (x^2 - 2x x_0 + x_0^2 + d^2) = n_1^2 (x^2 - 2x x_0 + x_0^2)(x_0^2 + h^2)$$

Set equal to zero and organize into powers of x_0

$$\begin{aligned}
&(n_1^2 - n_0^2) x_0^4 \\
&+ 2x(n_0^2 - n_1^2) x_0^3 \\
&+ [(n_1^2 - n_0^2)x^2 + (n_1^2 h^2 - n_0^2 d^2)] x_0^2 \\
&- (2n_1^2 x h^2) x_0 \\
&+ n_1^2 x^2 h^2 = 0
\end{aligned}$$

This will result in four roots. The unique solution is the one that is real, non-negative, and less than or equal to x.

Finally

$$r_0 = tan\left(\frac{x_0}{z_0}\right) \quad r_1 = tan\left(\frac{x_1}{z_1}\right)$$

where

$$z_0 = h, z_1 = d$$

SAR Aperture Length/Along-track Resolution

We want a specific along-track resolution at a certain depth below the air-ice interface. We know the SAR aperture length for a single medium from.

$$L = \frac{\lambda R}{2r_a}$$

To extrapolate to two-media we start with the medium containing the target (or source depending on your perspective.)

$$2x_1 = \frac{\lambda z_1}{2r_a}$$

We can get the angle θ_1 from simple trigonometry

$$\theta_1 = \tan^{-1}\left(\frac{x_1}{z_1}\right)$$

We can get θ_0 from Snell's Law

$$\theta_0 = \sin^{-1}\left(\frac{n_1}{n_0} sin(\theta_1)\right)$$

Some more trigonometry

$$x_0 = z_0 tan(\theta_0)$$

Finally, the SAR aperture length for a two-media model is just $L = 2x_0$

Putting this all together

$$L(r_a) = 2z_0 tan\left(\sin^{-1}\left(\frac{n_1}{n_0}\tan^{-1}\left(\frac{\lambda}{4r_a}\right)\right)\right)$$

Appendix C: ADC Shifting Example

For example if we had four consecutive records with a maximum signal value, after quantization, of 2^{14}-1 (16383, bin(11111111111111), largest possible output from the ADC). The first round of addition results in two records with maximum values of $2*(2^{14}-1) = 2^{15}-2$ (32766, bin(111111111111110)). These values can still be written as 16-bit unsigned integers. The second round of addition results in one record with a maximum value of 2^{16} (65536, bin((1)0000000000000000)) which is larger than the largest value possible to write as a 16-bit unsigned integer (65535, bin(1111111111111111)). In this case all the bits will be

rec1 = 16384, bin(0100000000000000)
rec2 = 16384, bin(0100000000000000)
rec3 = 16384, bin(0100000000000000)
rec4 = 16384, bin(0100000000000000)
rec1 + rec2 = rec12 = 32768, bin(1000000000000000)
rec3 + rec4 = rec34 = 32768, bin(1000000000000000)
rec12 + rec34 = rec1234 = 65536, bin((1)0000000000000000) Too big!
All bits get shifted to the right one space.
rec1234 = 32768, bin(1000000000000000)

The one in the right-most space (least significant bit) is truncated in favor of the value in entering the left-most space (most significant bit)

Appendix D: Matched Filter Derivation Via Maximum Likelihood Estimator

Let our observed signal be $\bar{x} = \bar{\bar{G}}\bar{s} + \bar{n}$

where $\bar{\bar{G}}$ *is the steering vector matrix*

$\bar{s}$ *is the signal of interest*

$\bar{n}$ *is the noise vector with correlation matrix* $\bar{\bar{C}}$

Let $\hat{s} = w^H x$ where w^H is a vector of weights

The multivariate Gaussian function for the MLE is

$$f_x(x) = \frac{1}{\pi^N |C|} \exp[-(x - Gs)^H C^{-1}(x - Gs)]$$

We want to maximize $f_x(x)$. To simplify matters we can take the log of both sides.

$$L_x = -N \log_{10} \pi - \log_{10}|C| - (x - Gs)^H C^{-1}(x - Gs)$$

We will be taking the gradient later so we can ignore all terms that are not dependent on s^H. We will also multiply by -1 and turn this from a maximization to a minimization problem. Applying these changes to $L_x$we get L'_x

$$L'_x = -s^H G^H C^{-1} x + s^H G^H C^{-1} Gs$$

Take the gradient with respect to s^H [5]. s now becomes the estimator $\hat{s}$.

$$\nabla_{s^H} L'_x = -G^H C^{-1} x + G^H C^{-1} G\hat{s} = 0$$

Solve for $\hat{s}$

$$\hat{s} = \frac{G^H C^{-1} x}{G^H C^{-1} G}$$

Since we are only estimating one signal G can be written as g

$$\hat{s} = \frac{g^H C^{-1} x}{g^H C^{-1} g}$$

Apply the Hermitian transform twice to $g^H C^{-1}$

$$\hat{s} = \frac{(C^{-1} g)^H x}{g^H C^{-1} g}$$

Since the equation is $\hat{s} = w^H x$

$$w = \frac{C^{-1}g}{g^H C^{-1} g}$$

These weights w will combine the elements of the observed signal x to create the maximum signal-to-noise ratio in the estimated signal $\hat{s}$.

Proof of Matched Filter as the Filter to Maximize SNR

Let our observed signal be $\bar{x} = \bar{\bar{G}}\bar{s} + \bar{n}$

where $\bar{\bar{G}}$ *is the steering vector matrix* (*this includes any system effects like heterogeneous SNR on different receivers*)

$\bar{s}$ *is the signal of interest*

$\bar{n}$ *is the noise vector with correlation matrix* $\bar{\bar{C}} = E\{nn^H\}$

Our matched filter is $w = \frac{C^{-1}g}{g^H C^{-1} g}$ or $w^H = \frac{g^H C^{-1}}{g^H C^{-1} g}$

SNR after filtering is

$$SNR = \frac{(w^H gs)^H (w^H gs)}{E\{(w^H n)^H (w^H n)\}}$$

Substitute in w^H. The denominators $\frac{1}{g^H C^{-1} g}$ cancel leaving

$$SNR = \frac{(g^H C^{-1} gs)^H (g^H C^{-1} gs)}{E\{(g^H C^{-1} n)^H (g^H C^{-1} n)\}}$$

Switch the order of the scalars in the denominator. Recall $C^{-H} = C^{-1}$.

$$SNR = \frac{(g^H C^{-1} g)^2 |s|^2}{E\{(g^H C^{-1} n)(g^H C^{-1} n)^H\}}$$

$$SNR = \frac{(g^H C^{-1} g)^2 |s|^2}{E\{g^H C^{-1} n n^H C^{-1} g\}}$$

The expectation is a linear operator so can go inside matrix multiplication

$$SNR = \frac{(g^H C^{-1} g)^2 |s|^2}{g^H C^{-1} E\{nn^H\} C^{-1} g}$$

$$SNR = g^H C^{-1} g |s|^2$$

$$\widehat{SNR} = g^H C^{-1} g |\hat{s}|^2$$

Special Case 1: Noise is Independent and Identically Distributed

If the noise is iid then the covariance matrix is just the noise variance multiplied by the identity matrix. This means the

$$\boldsymbol{C^{-1}} = \frac{1}{\sigma^2}\boldsymbol{I}$$

$$\boldsymbol{w} = \frac{\boldsymbol{I g} \sigma^2}{\boldsymbol{g}^H \boldsymbol{I g} \sigma^2}$$

$$\boldsymbol{w} = \frac{\boldsymbol{g}}{\boldsymbol{g}^H \boldsymbol{g}} = \frac{\boldsymbol{g}}{\|\boldsymbol{g}\|}$$

$$\hat{\boldsymbol{s}} = \frac{\boldsymbol{g}^H}{\|\boldsymbol{g}\|}\boldsymbol{x}$$

$$\widehat{SNR} = \frac{\|\boldsymbol{g}\| |\hat{\boldsymbol{s}}|^2}{\sigma^2}$$

Special Case 2: Noise is Independent but Not Identically Distributed

$$C = \begin{bmatrix} \sigma_1^2 & 0 & 0 \\ 0 & \sigma_2^2 & 0 \\ 0 & 0 & \sigma_3^2 \end{bmatrix}$$

$$w = \frac{C^{-1} g}{g^H C^{-1} g}$$

$$\widehat{SNR} = g^H C^{-1} g |\hat{s}|^2$$

Appendix E: Reference Coordinate Systems and Conversions

Local Reference Frame:

Body Coordinate System:
+x: out the noise of the aircraft
+y: out right wing
+z: local up & orthogonal to x
0: center of aircraft

Flight Coordinate System:
+x: direction of travel
+z: local up & orthogonal to x
+y: completes right handed coordinate system
0: first point of travelled path

Earth-Centered Earth-fixed:
+x: passes through equator at the prime meridian
+z: passes through north pole
+y: completes right handed coordinate system
0: center of Earth
The ECEF system is a Cartesian coordinate system with the origin at the Earth's center of mass. It axes are aligned with the International Reference Pole and International Reference Meridian.

WGS84 (Geodetic System):
Latitude: angle above or below the Equator (0°) extending to ±90°
Longitude: angle to the east or west of the Prime Meridian (0°) extending to ±180°
Elevation: height above the reference geoid in meters
WGS84 is, globally, the most accurate geodetic model of the earth. It includes

North-East-Down (NED):
+x: due north for the local reference frame
+y: due east for the local reference frame
+z: perpendicular to the local vertical pointing towards the center of the Earth
0: Center of aircraft

East-North-Up (ENU):
+x: due east for the local reference frame
+y: due north for the local reference frame
+z: perpendicular to the local vertical pointing away from the center of the Earth
0: Center of aircraft

Appendix F: Simulated P3 Antenna Array Pattern

Simulated results for the inboard P3 antenna array created by Emily Arnold.

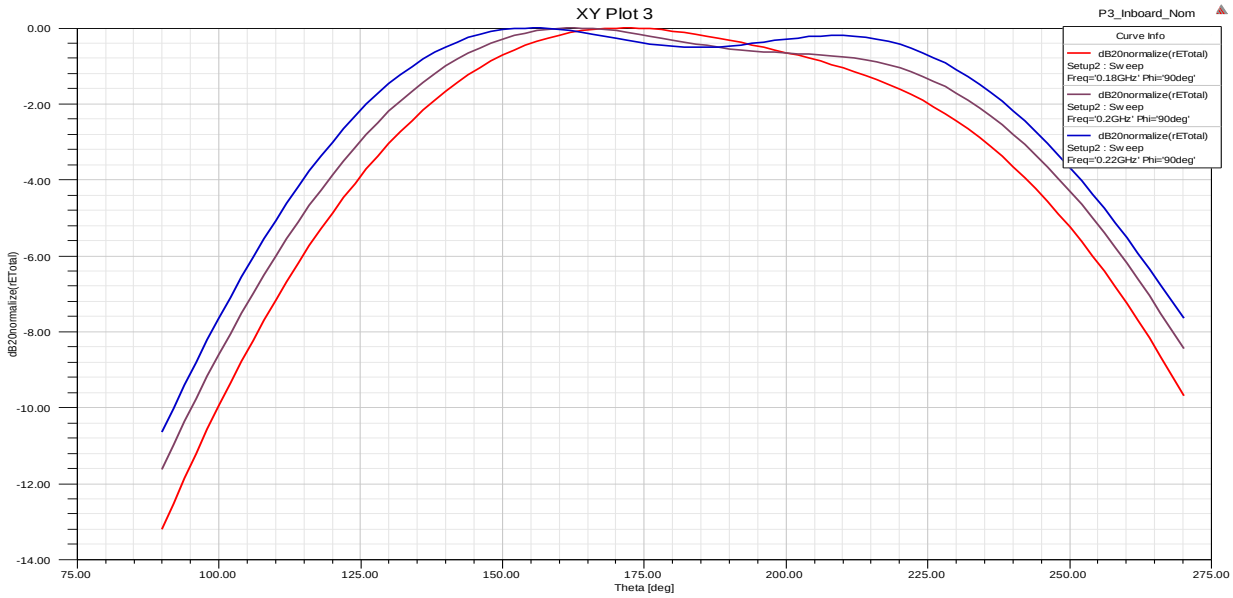

Appendix G: SAR aperture length versus SNR

Let there be a single along-track resolution cell coming from a SAR aperture of length such that there are $\frac{N}{2}$ independent samples. We split this single resolution cell into halves in the along-track dimension. The cells being half the width, will require a SAR aperture length such that there are N independent samples. Define two new vectors as

$$\bar{s}_1 : matched\ filter\ for\ the\ middle\ of\ pixel\ one$$

$$\bar{s}_2 : matched\ filter\ for\ the\ middle\ of\ pixel\ two$$

Defining $\otimes$ to be the standard Euclidean inner product, we therefore have,

$$\bar{s}_1 \otimes s_1 = N$$

$$\bar{s}_2 \otimes s_2 = N$$

$$\bar{s}_1 \otimes s_2 = 0$$

Let the noise power in each of the N samples be

$$P_{N_i} = \sigma_i^2 = \sigma^2 \ \ \forall i \in 1 \cdots N.$$

Define the scattering from each small pixel as:

α, β: two independent random variables associated with the signal of pixels one and two respectively

$$E\{\alpha^2\} = 1, \qquad E\{\beta^2\} = 1, \qquad E\{\alpha\beta\} = 0$$

Now take the first $\frac{N}{2}$ samples from $\bar{s}_1$ and $\bar{s}_2$ and define these new vectors:

$$\bar{s}_{11} : portion\ of\ s_1\ correlating\ with\ the\ shorter\ SAR\ aperture$$

$$\bar{s}_{21} : portion\ of\ s_2\ correlating\ with\ the\ shorter\ SAR\ aperture$$

Since they only use the first $\frac{N}{2}$ samples, we will have the following (approximately)

$$\bar{s}_{11} \otimes s_{11} = \frac{N}{2}$$

$$\bar{s}_{21} \otimes s_{11} = \frac{N}{2}.$$

For the SAR focusing with the smaller aperture, we can use $\bar{s}_{11}$ as the matched filter for our image pixel. The total noise power in the image pixel after matched filtering is

$$P_N = \sum_{i=0}^{\frac{N}{2}} \sigma_i^2 = \frac{N}{2}\sigma^2$$

because the noise power sums incoherently. The signal is the inner product

$$(\bar{s}_{11} \cdot \alpha + \bar{s}_{21} \cdot \beta).* s_{11}$$

$$\frac{N}{2} \cdot \alpha + \frac{N}{2} \cdot \beta.$$

When converting to expected power, since $E\{\alpha^2\} = E\{\beta^2\} = 1$ and they are orthogonal

$$P_S = (E\{\alpha^2\} + E\{\beta^2\}) \cdot \frac{N^2}{4} = \frac{N^2}{2}.$$

Then the SNR is

$$SNR_{\frac{N}{2}} = \frac{P_S}{P_N} = \frac{\frac{N^2}{2}}{\frac{N\sigma^2}{2}} = \frac{N}{\sigma^2}$$

If we then double the SAR aperture to include N independent samples, the resolution cell size is halved. The noise power is now

$$P_N = \sum_{i=0}^{N} \sigma_i^2 = N\sigma^2$$

and the signal is the inner product

$$(s_1 \cdot \alpha + s_2 \cdot \beta).* s_1.$$

However, since $\bar{s}_1$ and $\bar{s}_2$ are orthogonal by nature, then

$$(\bar{s}_1 \otimes s_1) \cdot \alpha = N \cdot \alpha.$$

When converted to power we get

$$P_S = N^2 E\{\alpha^2\} = N^2$$

Then the SNR is

$$SNR_N = \frac{P_S}{P_N} = \frac{N^2}{N\sigma^2} = \frac{N}{\sigma^2}.$$

Thus we see that

$$SNR_{\frac{N}{2}} = SNR_N = \frac{N}{\sigma^2}.$$

This means the SNR is constant versus SAR aperture length as long as the target energy is distributed evenly in the pixel.